Inorg. Chem. **2007**, *46*, 3889–3902

Further Insights into the Spectroscopic Properties, Electronic Structure, and Kinetics of Formation of the Heme–Peroxo–Copper Complex $[(F_8TPP)Fe^{III}–(O_2^{2-})–Cu^{II}(TMPA)]^+$

Reza A. Ghiladi,[†,£] Eduardo E. Chufán,[†] Diego del Río,[‡] Edward I. Solomon,[‡] Carsten Krebs,[§,#] Boi Hanh Huynh,[§] Hong-wei Huang,[||] Pierre Moënne-Loccoz,[||] Susan Kaderli,[⊥] Marcus Honecker,[⊥] Andreas D. Zuberbühler,[⊥] Lisa Marzilli,[▽] Robert J. Cotter,[▽] and Kenneth D. Karlin*[,†]

Department of Chemistry, The Johns Hopkins University, Charles and 34th Streets, Baltimore, Maryland 21218, Department of Chemistry, Stanford University, Stanford, California 94305, Department of Physics, Emory University, Atlanta, Georgia 30322, Department of Environmental & Biomolecular Systems, OGI School of Science and Engineering, Oregon Health and Science University, Beaverton, Oregon 97006, Department of Chemistry, University of Basel, CH-4056 Basel, Switzerland, and Department of Pharmacology and Molecular Sciences, The Johns Hopkins School of Medicine, Baltimore, Maryland 21205

Received September 12, 2006

In the further development and understanding of heme–copper O_2-reduction chemistry inspired by the active-site chemistry in cytochrome *c* oxidase, we describe a dioxygen adduct, $[(F_8TPP)Fe^{III}–(O_2^{2-})–Cu^{II}(TMPA)](ClO_4)$ (**3**), formed by addition of O_2 to a 1:1 mixture of the porphyrinate–iron(II) complex $(F_8TPP)Fe^{II}$ (**1a**) {F_8TPP = tetrakis-(2,6-difluorophenyl)porphyrinate dianion} and the copper(I) complex $[(TMPA)Cu^{I}(MeCN)](ClO_4)$ (**1b**) {TMPA = tris-(2-pyridylmethyl)amine}. Complex **3** forms in preference to heme-only or copper-only binuclear products, is remarkably stable {$t_{1/2}$ (RT; MeCN) $\approx$ 20 min; λ_{max} = 412 (Soret), 558 nm; EPR silent}, and is formulated as a peroxo complex on the basis of manometry {**1a**/**1b**/O_2 = 1:1:1}, MALDI-TOF mass spectrometry {$^{16}O_2$, *m*/*z* 1239 [(**3** + MeCN)$^+$]; $^{18}O_2$, *m*/*z* 1243}, and resonance Raman spectroscopy {$\nu_{(O-O)}$ = 808 cm^{-1}; $\Delta^{16}O_2/^{18}O_2$ = 46 cm^{-1}; $\Delta^{16}O_2/^{16/18}O_2$ = 23 cm^{-1}}. Consistent with a μ-η^2:η^1 bridging peroxide ligand, two metal–O stretching frequencies are observed {$\nu_{(Fe-O)}$ = 533 cm^{-1}, $\nu_{(Fe-O-Cu)}$ = 511 cm^{-1}}, and supporting normal coordinate analysis is presented. ^2H and ^{19}F NMR spectroscopies reveal that **3** is high-spin {also μ_B = 5.1 ± 0.2, Evans method} with downfield-shifted pyrrole and upfield-shifted TMPA resonances, similar to the pattern observed for the structurally characterized μ-oxo complex $[(F_8TPP)Fe^{III}–O–Cu^{II}(TMPA)]^+$ (**4**) (known *S* = 2 system, antiferromagnetically coupled high-spin Fe^{III} and Cu^{II}). Mössbauer spectroscopy exhibits a sharp quadrupole doublet (zero field; δ = 0.57 mm/s, $|\Delta E_Q|$ = 1.14 mm/s) for **3**, with isomer shift and magnetic field dependence data indicative of a peroxide ligand and *S* = 2 formulation. Both UV–visible-monitored stopped-flow kinetics and Mössbauer spectroscopic studies reveal the formation of heme-only superoxide complex $(S)(F_8TPP)Fe^{III}–(O_2^-)$ (**2a**) (S = solvent molecule) prior to **3**. Thermal decomposition of μ-peroxo complex **3** yields μ-oxo complex **4** with concomitant release of ~0.5 mol O_2 per mol **3**. Characterization of the reaction **1a**/**1b** + $\mathbf{O_2}$ → **2** → **3** → **4**, presented here, advances our understanding and provides new insights to heme/Cu dioxygen-binding and reduction.

Introduction

As a member of the heme−copper oxidase superfamily, cytochrome *c* oxidase (C*c*O) utilizes electrons provided sequentially by cytochrome *c* to catalyze the $4e^-/4H^+$ reduction of dioxygen to water.[1−9] This membrane-bound multimetallic enzyme couples this exergonic process to the movement of four additional protons across the mitochondrial membrane, resulting in a net translocation of four charges. The proton pumping mechanism of C*c*O generates the

* To whom correspondence should be addressed. E-mail: karlin@jhu.edu.
[†] Department of Chemistry, The Johns Hopkins University.
[‡] Stanford University.
[§] Emory University.
[||] Oregon Health and Science University.
[⊥] University of Bazel.
[▽] Department of Pharmacology and Molecular Sciences, The Johns Hopkins University.
[#] Current address: Department of Chemistry, Pennsylvania State University, University Park, PA 16802.
[£] Current address: Department of Chemistry, North Carolina State University, Raleigh, NC 27695.

(1) Ferguson-Miller, S.; Babcock, G. T. *Chem. Rev.* **1996**, *96*, 2889−2907.
(2) Michel, H.; Behr, J.; Harrenga, A.; Kannt, A. *Annu. Rev. Biophys. Biomol. Struct.* **1998**, *27*, 329−356.
(3) Kitagawa, T. *J. Inorg. Biochem.* **2000**, *82*, 9−18.
(4) Collman, J. P.; Boulatov, R.; Sunderland, C. J. *Porphyrin Handbook* **2003**, *11*, 1−49.
(5) Kim, E.; Chufán, E. E.; Kamaraj, K.; Karlin, K. D. *Chem. Rev.* **2004**, *104*, 1077−1133.

10.1021/ic061726k CCC: $37.00
Published on Web 04/20/2007

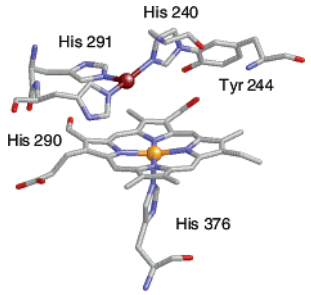

Figure 1. Rasmol depiction of the heme a_3-Cu_B binuclear active site of dioxygen reduction from bovine cytochrome *c* oxidase. Coordinates (1OCR) were obtained from the Protein Data Bank (Brookhaven, NY).[13]

membrane potential used by ATP synthase to drive the formation of ATP from ADP, and in light of its biologically important relevance, has been the subject of numerous and intense biophysical and spectroscopic investigations.

Confirming earlier biochemical and molecular biological suppositions are the recent X-ray crystallographic studies which show that dioxygen reduction occurs at an active site consisting of a heme a_3-Cu_B heterobinuclear center with an intermetal separation of 4.5−5.2 Å, depending on the protein derivative (Figure 1).[5−9] As it is generally considered, dioxygen binding and reduction occurs as follows:[5,10−12] An initial Cu_B-O_2 interaction precedes transfer of O_2 to heme a_3, forming a ferrous−oxy (Fe^{III}−superoxo) observable intermediate (**A**). The next intermediate detected has already undergone O−O cleavage, giving the ferryl Fe^{IV}═O species (**P**) and Cu_B^{II}−OH, with either tyrosinate or tyrosyl radical ($Tyr^{\bullet}$), depending on the enzyme form used for the O_2-chemistry. Rapid O−O cleavage seems an attractive mechanistic feature as such a reaction course bypasses the formation of potentially cytotoxic (if leaked) superoxide (as O_2^- or HO_2) or peroxide (as HO_2^- or H_2O_2) products. However, (hydro)peroxide metal-bridged or associated $Fe^{III}-O-O(H)\cdots Cu_B$ transients or intermediates have also been discussed, based on structural, spectroscopic, and theoretical considerations.[5,7,13,14] The post-translationally formed amino-acid His−Tyr cross-link (Figure 1)[5,15] may be key in the reduction mechanism as a hydrogen atom (i.e., proton plus

Chart 1

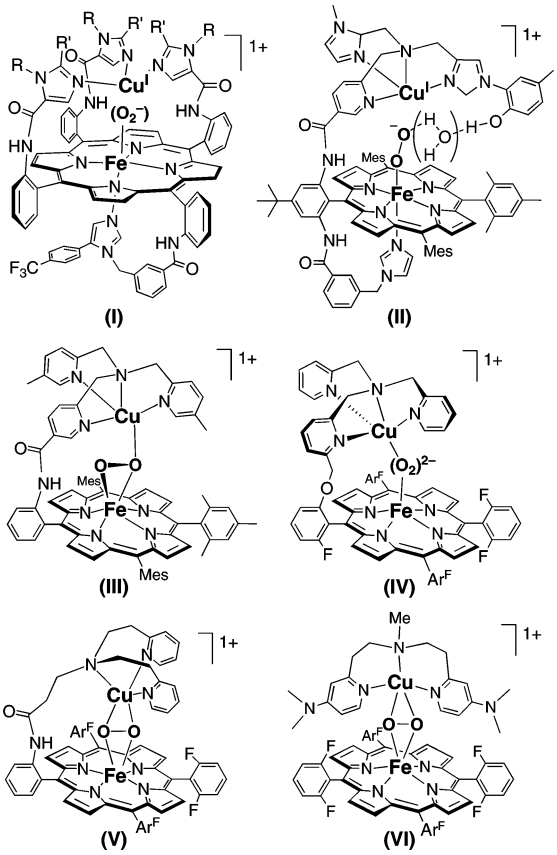

electron) donor, and/or as an important element of the proton-pumping mechanism. Despite the wealth of knowledge, complete insights are lacking, including a full understanding of the nature of O_2-intermediates (and their protonation states) forming prior to the O−O cleavage process.

There has also been intense interest from inorganic chemists to provide coordination chemistry insights into C*c*O heme a_3-Cu_B physical properties and reactivity. Dioxygen reactivity studies have recently undergone considerable advancement, as approached either via electrocatalytic O_2-reduction with heme−Cu assemblies[4,16] or by the generation of O_2-adducts of discrete heme−Cu complexes or heme and Cu−ligand components.[5,17] Some recent examples are given in Chart 1. Collman[18] and more recently Naruta[19] have generated heme−superoxide ($Fe^{III}-O_2^-$) moieties, **I** and **II**, respectively, which are stable in the presence of the neighboring Cu(I) complex; these species mimic the formation of the initial O_2-adduct **A** intermediate in the C*c*O O_2-reduction cycle. Likewise, we have spectroscopically and/or kinetically observed solutions containing both $Fe-O_2$ and Cu^I species which exist prior to forming μ-peroxo $Fe^{III}-(O_2^{2-})-Cu^{II}$ products.[20−25] An exciting development was Naruta's crystal structure determination of binuclear complex

(6) Kannt, A.; Michel, H. Bacterial cytochrome *c* oxidase. In *Handbook of Metalloproteins*; Messerschmidt, A, Huber, R., Poulos T., Wieghardt, K., Eds.; Wiley: New York, 2001; Vol. 1; pp 331−347.
(7) Yoshikawa, S. *Adv. Protein Chem.* **2002**, *60*, 341−395.
(8) Yoshikawa, S.; Shinzawa-Itoh, K.; Yamashita, E.; Tsukihara, T. Mitochodrial cytochrome *c* oxidase. In *Handbook of Metalloproteins*; Messerschmidt, A, Huber, R., Poulos T., Wieghardt, K., Eds.; Wiley: New York, 2001; Vol. 1; pp 348−362.
(9) Than, M. E.; Tewfik, S. *ba*$_3$-Cytochrome *c* oxidase from *Thermus thermophilus*. In *Handbook of Metalloproteins*; Messerschmidt, A, Huber, R., Poulos T., Wieghardt, K., Eds.; Wiley: New York, 2001; Vol. 1; pp 363−378.
(10) Babcock, G. T. *Proc. Natl. Acad. Sci. U.S.A.* **1999**, *96*, 12971−12973.
(11) Brunori, M.; Giuffre, A.; Sarti, P. *J. Inorg. Biochem.* **2005**, *99*, 324−336.
(12) Barry, B. A.; Einarsdottir, O. *J. Phys. Chem. B* **2005**, *109*, 6972−6981.
(13) Yoshikawa, S.; Shinzawa-Itoh, K.; Nakashima, R.; Yaono, R.; Yamashita, E.; Inoue, N.; Yao, M.; Jei-Fei, M.; Libeu, C. P.; Mizushima, T.; Yamaguchi, H.; Tomizaki, T.; Tsukihara, T. *Science* **1998**, *280*, 1723−1729.
(14) Blomberg, M. R. A.; Siegbahn, P. E. M.; Wikström, M. *Inorg, Chem.* **2003**, *42*, 5231−5243.
(15) Buse, G.; Soulimane, T.; Dewor, M.; Meyer, H. E.; Blüggel, M. *Protein Sci.* **1999**, *8*, 985−990.
(16) Collman, J. P.; Boulatov, R.; Sunderland, C. J.; Fu, L. *Chem. Rev.* **2004**, *104*, 561−588.
(17) Karlin, K. D.; Kim, E. *Chem. Lett.* **2004**, *33*, 1226−1231.
(18) Collman, J. P.; Sunderland, C. J.; Berg, K. E.; Vance, M. A.; Solomon, E. I. *J. Am Chem. Soc.* **2003**, *125*, 6648−6649.
(19) Liu, J. G.; Naruta, Y.; Tani, F. *Angew. Chem., Int. Ed.* **2005**, *44*, 1836−1840.

(**III**) demonstrating that an η^2:η^1 Fe^{III}−(O$_2^{2-}$)−Cu^{II} coordination is a viable structure, at least in a high-spin complex.[26] These systems employ binucleating superstructured ligands, i.e., hemes with covalently linked chelates for copper. We have also studied closely related systems, including O$_2$-adducts which lead to high-spin μ-peroxo Fe^{III}−(O$_2^{2-}$)−Cu^{II} complexes [(^{6}L)Fe^{III}−(O$_2^{2-}$)−Cu^{II}]$^+$ (**IV**)[20,22] and [(^{2}L)Fe^{III}−(O$_2^{2-}$)−Cu^{II}]$^+$ (**V**).[23,24] In combination, studies on these complexes reveal that the O−O bond strength (as indicated by ν_{O-O}) can be dramatically lowered (by ∼40−50 cm^{-1}) by changing the peroxo-binding from a tetradentate to tridentate Cu-chelate and this also changes the peroxo structure to μ-η^2:η^2 as observed for complex **V**,[23,24] and also for an 'untethered' analogue **VI** (Chart 1).[25]

Thus, such investigations involving systematic changes in heme/Cu ligand environment provide insight into the O$_2$-binding process and properties of the resulting new types of dioxygen adducts. To these ends, we have also studied heme/Cu/O$_2$ chemistry of the 1:1 mixture of (F$_8$TPP)Fe^{II} (**1a**)[27] and [(TMPA)Cu^{I}(MeCN)]$^+$ (**1b**)[28−30] (Scheme 1). As a close analogue of [(^{6}L)Fe^{III}−(O$_2^{2-}$)−Cu^{II}]$^+$ (**IV**) (Chart 1), we reported the preliminary characterization of the high-spin heme/Cu μ-peroxo complex, [(F$_8$TPP)Fe^{III}−(O$_2^{2-}$)−Cu^{II}(TMPA)]$^+$ (**3**),[21] which forms in lieu of heme-only or Cu-only products prior to its thermal transformation to the structurally characterized μ-oxo species [(F$_8$TPP)Fe^{III}−O−Cu^{II}(TMPA)]$^+$ (**4**).[31] Deeper insights in the structure of peroxo complex **3** have recently come from both X-ray absorption spectroscopy (i.e., EXAFS) and DFT calculations,[32] showing that the bound peroxide assumes a μ-η^2:η^1 geometry like that of Naruta's complex (**III**, Chart 1). The computational work also reveals insights into the bonding in **3** and the magnetic orbitals which mediate the antiferromagnetic coupling between the high-spin iron(III) heme and the Cu(II)−TMPA moiety via the peroxide bridging ligand.[32]

Scheme 1

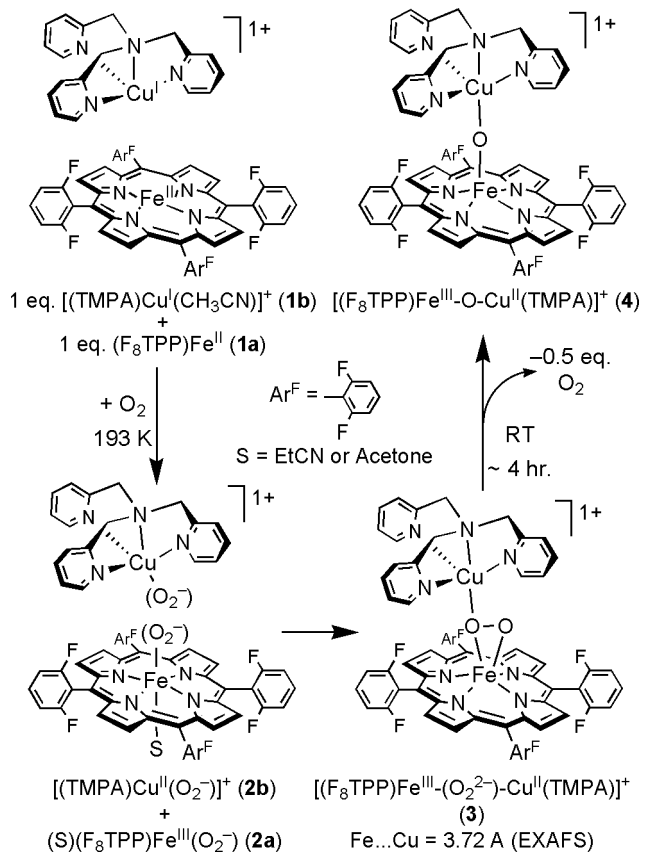

The focus of this report is to provide a completed picture for the chemistry of **3** and of its formation (Scheme 1) with results and experimental details *not* previously described: (i) new resonance Raman spectroscopic measurements reveal the presence of two inequivalent metal−oxo stretching vibrations consistent with the η^2:η^1 peroxo bridging structure deduced from EXAFS spectroscopic and computational results,[32] (ii) ^{2}H NMR spectroscopy employing a deuterated F$_8$TPP porphyrinate illustrates the clean direct reduced-to-peroxo-to-oxo complex conversion and ^{19}F NMR spectroscopy provides additional new characterization of the system, (iii) new Mössbauer spectroscopic measurements provide parameters which define the system and provide insights into the electronics/bonding of [(F$_8$TPP)Fe^{III}−(O$_2^{2-}$)−Cu^{II}(TMPA)]$^+$ (**3**), and a detailed analysis is provided, and (iv) dynamics information is provided via low-temperature stopped-flow kinetics for the reduced-to peroxo conversion in EtCN as solvent. The combination of the kinetic studies and Mössbauer spectroscopy further provides unequivocal evidence for the presence of a heme−superoxo intermediate, (solvent)(F$_8$TPP)Fe^{III}−(O$_2^{-}$) (**2a**, Scheme 1) formed prior to the formation of **3**.

(20) Ghiladi, R. A.; Huang, H. W.; Moënne-Loccoz, P.; Stasser, J.; Blackburn, N. J.; Woods, A. S.; Cotter, R. J.; Incarvito, C. D.; Rheingold, A. L.; Karlin, K. D. *J. Biol. Inorg. Chem.* **2005**, *10*, 63−77.

(21) Ghiladi, R. A.; Hatwell, K. R.; Karlin, K. D.; Huang, H.-w.; Moënne-Loccoz, P.; Krebs, C.; Huynh, B. H.; Marzilli, L. A.; Cotter, R. J.; Kaderli, S.; Zuberbühler, A. D. *J. Am. Chem. Soc.* **2001**, *123*, 6183−6184.

(22) Ghiladi, R. A.; Ju, T. D.; Lee, D.-H.; Moënne-Loccoz, P.; Kaderli, S.; Neuhold, Y.-M.; Zuberbühler, A. D.; Woods, A. S.; Cotter, R. J.; Karlin, K. D. *J. Am. Chem. Soc.* **1999**, *121*, 9885−9886.

(23) Kim, E.; Helton, M. E.; Lu, S.; Moënne-Loccoz, P.; Incarvito, C. D.; Rheingold, A. L.; Kaderli, S.; Zuberbühler, A. D.; Karlin, K. D. *Inorg, Chem.* **2005**, *44*, 7014−7029.

(24) Kim, E.; Shearer, J.; Lu, S.; Moënne-Loccoz, P.; Helton, M. E.; Kaderli, S.; Zuberbühler, A. D.; Karlin, K. D. *J. Am Chem. Soc.* **2004**, *126*, 12716−12717.

(25) Kim, E.; Helton, M. E.; Wasser, I. M.; Karlin, K. D.; Lu, S.; Huang, H.-w.; Moënne-Loccoz, P.; Incarvito, C. D.; Rheingold, A. L.; Honecker, M.; Kaderli, S.; Zuberbühler, A. D. *Proc. Natl. Acad. Sci. U.S.A.* **2003**, *100*, 3623−3628.

(26) Chishiro, T.; Shimazaki, Y.; Tani, F.; Tachi, Y.; Naruta, Y.; Karasawa, S.; Hayami, S.; Maeda, Y. *Angew. Chem., Int. Ed.* **2003**, *42*, 2788−2791.

(27) Ghiladi, R. A.; Kretzer, R. M.; Guzei, I.; Rheingold, A. L.; Neuhold, Y.-M.; Hatwell, K. R.; Zuberbühler, A. D.; Karlin, K. D. *Inorg. Chem.* **2001**, *40*, 5754−5767.

(28) Tyeklár, Z.; Jacobson, R. R.; Wei, N.; Murthy, N. N.; Zubieta, J.; Karlin, K. D. *J. Am. Chem. Soc.* **1993**, *115*, 2677−2689.

(29) Karlin, K. D.; Lee, D.-H.; Kaderli, S.; Zuberbühler, A. D. *Chem. Commun.* **1997**, 475−476.

(30) Karlin, K. D.; Kaderli, S.; Zuberbühler, A. D. *Acc. Chem. Res.* **1997**, *30*, 139−147.

(31) Karlin, K. D.; Nanthakumar, A.; Fox, S.; Murthy, N. N.; Ravi, N.; Huynh, B. H.; Orosz, R. D.; Day, E. P. *J. Am. Chem. Soc.* **1994**, *116*, 4753−4763.

(32) del Rio, D.; Sarangi, R.; Chufán, E. E.; Karlin, K. D.; Hedman, B.; Hodgson, K. O.; Solomon, E. I. *J. Am. Chem. Soc.* **2005**, *127*, 11969−11978.

Experimental Procedures

Materials and Methods. $(F_8TPP)Fe^{II}$ (**1a**),[27,33] $(F_8TPP\text{-}d_8)Fe^{II}$ (**1a-*d*$_8$**),[27,33] and $[(TMPA)Cu^{I}(MeCN)](ClO_4)$ (**1b**)[28] were prepared per literature precedent. $(F_8TPP)^{57}Fe^{II}$ (**1a-^{57}Fe**) was prepared in an identical manner to **1a**, but employing $^{57}Fe^{II}Cl_2$ (see Supporting Information) in lieu of $Fe^{II}Cl_2$. Ultrapure grade dioxygen (99.994%, WSC Gas), breakseal flasks of $^{18}O_2$ and $^{16/18}O_2$ (Icon Stable Isotopes), and ^{57}Fe metal (95.3%, AMT) were purchased as indicated. All other reagents and solvents were purchased from commercial sources and were of available reagent quality unless otherwise stated. Acetonitrile (MeCN) was distilled directly from CaH_2 under argon and stored over molecular sieves. Solvents and solutions were deoxygenated by either repeated freeze−pump−thaw cycles (5×), or by bubbling of argon (>25 min) directly through the solution. Solid samples were stored and transferred, and samples for spectroscopic characterization were prepared in an MBraun LabMaster 130 inert atmosphere (<1 ppm O_2, <1 ppm H_2O) glovebox under nitrogen atmosphere.

NMR spectra were measured on a Varian NMR instrument at 61 (^{2}H) or 376 MHz (^{19}F). Chemical shifts are reported as δ values calibrated to natural abundance deuterium solvent peaks (^{2}H) or as δ values referenced to an external standard of α,α,α-trifluorotoluene at −63.73 ppm (^{19}F). Low-temperature UV−visible spectral studies were performed on a Hewlett-Packard 8453A diode array spectrometer equipped with a variable-temperature dewar and cuvette assembly.[34,35] Molar extinction coefficients are reported as an average of a minimum of three trials.

Low-Temperature NMR Spectroscopy/Evans Method Magnetic Moment Measurements. Multinuclear (^{1}H, ^{2}H, and ^{19}F) NMR spectroscopic and magnetic moment measurements for **3** were performed as previously described for $[(^6L)Fe^{III}-(O_2^{2-})-Cu^{II}]$.[20] Measurements on the decomposition product **4** were accomplished by warming the NMR instrument to room temperature to facilitate decay of the dioxygen adduct (as monitored by NMR), followed by recooling and recording of the ^{1}H, ^{2}H NMR spectra at low temperature. Evans method data were analyzed using a nuclearity of **1** (i.e., one combined/coupled magnetic center) in the magnetic moment equations.[20]

Matrix-Assisted Laser Desorption Ionization Time-of-Flight Mass Spectrometry (MALDI-TOF-MS). MALDI-TOF-MS mass spectra were recorded on a Kratos Analytical Kompact MALDI 4 mass spectrometer equipped with a 337 nm nitrogen laser (20 kV extraction voltage). Initial calibration of the instrument was performed with a known standard (i.e., matrix) and then reconfirmed on known samples (i.e., F_8TPPH_2 or $(F_8TPP)Fe^{III}-OH$). In the glovebox, matrix-free samples were prepared upon addition of 20 mg of **1a**, 12 mg of **1b**, and 1 g of deoxygenated MeCN to a 10 mL Schlenk flask. A small aliquot of the solution was transferred via pipet to a MALDI-TOF-MS sample holder and allowed to evaporate, thereby adhering the sample to the target. For **3**, the remainder of the solution of **1a**/**1b** was removed from the glovebox, cooled to −45 °C (dry ice/MeCN cold bath), and oxygenated with an excess of either $^{16}O_2$ or $^{18}O_2$ (96.5 atom % ^{18}O or greater), affording the $^{16}O_2$ or $^{18}O_2$ heme−peroxo−Cu complexes, respectively. The dioxygen adducts were then transferred to sample holders as above, the solvent allowed to evaporate under an argon stream at room temperature, and immediately placed into the mass spectrometer.

Resonance Raman Spectroscopy of $[(F_8TPP)Fe^{III}-(O_2^{2-})-Cu^{II}(TMPA)](ClO_4)$ (3). 1a (20 mg) and 12 mg of **1b** were dissolved in 10 mL of deoxygenated MeCN in a glovebox. The resulting solution was divided into aliquots and transferred to septum-sealed NMR tubes (~0.5 mL per tube). As a control, one NMR tube was directly frozen in liquid N_2 and sealed under inert atmosphere. The remaining tubes were placed in a dry ice/MeCN cold bath, and oxygenated using (i) $^{16}O_2$, (ii) $^{18}O_2$ (95.0 atom % ^{18}O or greater), and (iii) mixed-isotope $^{16/18}O_2$ gas (1:2:1 of $^{16}O_2$/$^{16/18}O_2$/$^{18}O_2$). Oxygenations were performed using a 5 mL Hamilton gastight syringe equipped with a three-way syringe purge valve attached to an argon/vacuum line of a Schlenk manifold. The breakseal flasks containing the isotopically labeled O_2 were frozen in a dry ice/MeCN cold bath during the extraction of O_2 to freeze out any water contaminant. The oxygenated samples were frozen in liquid N_2 and sealed under their isotopically labelled O_2 atmosphere, thereby allowing the headspace of the samples to be checked directly by resonance Raman for their isotopic purity and consistency.

Resonance Raman (rR) spectra obtained at OHSU (P. M.-L.) resulted from 413-nm excitation as described previously.[20−25] rR spectroscopy with 676-nm excitation (E.I.S., Stanford University) was performed with a Princeton Instruments ST-135 back-illuminated CCD detector on a Spex 1877 CP triple monochromator with 1200, 1800, and 2400 grooves/mm holographic spectrograph gratings. Excitation was provided by a Coherent I90C-K Kr^+ ion laser. Samples were run at 77 K in a liquid N_2 finger Dewar (Wilmad).

Stopped-Flow Spectrophotometry. Preparation and handling of sample solutions of **1a** and **1b** (1:1 mixtures in reagent grade propionitrile), along with collection of data and analysis, were carried out as described for other heme and/or copper systems.[21,23,25,27] A total of 112 individual runs were used for the final calculations (cf. the Eyring plot supplied in the Supporting Information). Data collection times varied between 0.7 and 169 s in the temperature range of −90.4 to −65.1 °C.

Dioxygen Evolution from 3. An alkaline pyrogallol solution was used to detect if dioxygen was evolved upon the decomposition of **3** to **4** in a manner identical to published protocols[20,23] and as described in further detail in the Supporting Information. The number of equivalents of O_2 evolved were computed on the basis of a sample of **3** formed upon low-temperature oxygenation of $(F_8TPP)Fe^{II}/[(TMPA)Cu^{I}(MeCN)](ClO_4)$ {**1a**/**1b** = 40 mg/24 mg} in 10 mL of MeCN. The published calibration curve,[20] absorbance (400 nm) = (0.0716 × mL O_2) + 0.026, was used to determine the amount of O_2 released upon thermal decomposition of **3** to **4**. When **3** was formed with excess dioxygen, A_{400} measurements of the alkaline pyrogallol solution (0.208 and 0.216) revealed 0.43 and 0.45 equiv of O_2 generated, respectively. Formation of **3** with a stoichiometric addition of dioxygen led to an A_{400} of 0.194, corresponding to 0.40 equiv of dioxygen evolved.

Mössbauer Spectroscopy of 3. In the glovebox, to a 25 mL Schlenk flask equipped with stir bar was added 20 mg of **1a-^{57}Fe** and 12 mg of **1b** (1:1 mixture) in 10 mL of acetonitrile. Approximately 250 μL of this solution was transferred to a Mössbauer sample holder, placed in an airtight flask, and immediately frozen in liquid N_2 upon removal from the glovebox. The remainder of the solution was removed from the glovebox in the Schlenk flask, placed in a −40 °C dry ice/MeCN cold bath,

(33) Kopf, M.-A.; Neuhold, Y.-M.; Zuberbühler, A. D.; Karlin, K. D. *Inorg. Chem.* **1999**, *38*, 3093−3102.
(34) Karlin, K. D.; Haka, M. S.; Cruse, R. W.; Meyer, G. J.; Farooq, A.; Gultneh, Y.; Hayes, J. C.; Zubieta, J. *J. Am. Chem. Soc.* **1988**, *110*, 1196−1207.
(35) Karlin, K. D.; Cruse, R. W.; Gultneh, Y.; Farooq, A.; Hayes, J. C.; Zubieta, J. *J. Am. Chem. Soc.* **1987**, *109*, 2668−2679.

and oxygenated via direct O_2 bubbling, thereby forming **3**. This solution was then added by pipet to a Mössbauer sample holder prechilled over CO_2(s). The sample was then frozen and stored in liquid N_2 prior to data collection.

Mössbauer spectra were recorded either on a weak-field (50 mT removable permanent magnet) Mössbauer spectrometer equipped with a Janis 8 DT variable-temperature cryostat or on a strong-field Mössbauer spectrometer equipped with a Janis 12 CNDT/SC SuperVaritemp cryostat containing an 8-T superconducting magnet. Both spectrometers were operated in a constant acceleration mode in a transmission geometry. The zero velocity of the Mössbauer spectra is referred to the centroid of the room-temperature spectrum of a metallic iron foil. Both spectrometers were equipped with temperature controls that allow the sample to be stablilized at any temperature between 1.5 and 300 K.

Computational Details. Nomal coordinate analysis (NCA) was performed on a simplified Fe−O_2−Cu complex by using QCPE program 576 by M. R. Peterson and D. F. McIntosh, which involves solution of the secular equation $|\mathbf{FG} - \lambda\mathbf{E}| = 0$[36,37] by the diagonalization procedure of Miyazawa.[38] The calculations were based on a general valence force field. Force constants were refined with the nonlinear optimization routine of the simplex algorithm according to Nelder and Mead.[39] The input geometry was taken from DFT calculations. The mass of Fe and Cu atoms was increased to 103 and 101 g·mol^{-1}, respectively, to reflect the effects of the porphyrin and TMPA ligands on their displacements. Such an effective mass increase is necessary to properly reproduce experimental results. A similar approach has been used by us in the study of binuclear peroxo copper complexes containing the TMPA ligand.[40]

Density functional theory (DFT) calculations of the model complex [(P)Fe^{III}−(O_2^{2-})−Cu^{II}(TMPA)]$^+$ were performed using the Gaussian 98−03 package of programs[41] at the BP86 functional[42,43] using the 6-311G* basis set for Fe, Cu, and O, 6-31G* for N, and 6-31G for C and H. The structure was characterized as an energy minimum by diagonalization of the analytically computed Hessian (vibrational frequencies calculations). Molekel was used to visualize the results of DFT calculations.[44]

Results and Discussion

Dioxygen Reactivity of 1a/1b: UV−Visible Spectroscopy. As reported earlier,[21] upon bubbling of dioxygen directly through a 1:1 solution of **1a** and **1b** {λ_{max} (ϵ, mM^{-1} cm^{-1}) = 414 (145), 421 (Soret: 220), 526 (20.2) nm}, UV−visible spectroscopic monitoring in nitrile solvent revealed the irreversible formation of a new species {λ_{max} (ϵ, mM^{-1} cm^{-1}) = 412 (Soret: 112), 558 (12.5) nm} (Figure S1)[45] having remarkable thermal stability ($t_{1/2}$(RT) ≈ 20 min in MeCN), which we have formulated as the peroxo-level dioxygen adduct **3** (Scheme 1). When oxygenation was performed at low temperature, e.g., −40 °C for MeCN, the stability of **3** was increased to over 24 h. Thermal decomposition (RT) of **3** led to formation of the previously[31] structurally characterized μ-oxo complex **4** {λ_{max} (ϵ, mM^{-1} cm^{-1}) = 433 (Soret: 146), 553 (13.1) nm}.[46]

Consistent with the formulation of **3** as a μ-peroxo bridged heme−Cu complex (as depicted in Scheme 1) was the determination of the dioxygen uptake of **1a/1b** (1:1 mixture), utilizing a spectrophotometric titration methodology we have described;[20,23] further details are provided here.[45] As reported earlier,[21] full formation of **3** was accomplished with an overall oxygenation stoichiometry of 0.9−1.0 equiv O_2 per 1:1 mixture of **1a/1b**, suggesting the presence of an intramolecular O_2-adduct (Figure S2).[45] Furthermore, the UV−visible spectral features and oxygenation behavior of **3** are very similar to its tethered analogue **IV** (Chart 1) {λ_{max} = 418 (Soret), 561 nm, MeCN},[20,22] which has been shown to contain such a bound peroxide species.

While the oxygenation stoichiometry for formation of **3** is consistent with an intramolecular O_2-adduct, it alone does not completely rule out the possibility of a heme-only {i.e., (PFe^{III})$_n$−(O_2^{n-}), n = 1: 414−418 (Soret), 536−537 nm; n = 2: 414−418 (Soret), 535−536 nm}[27] or copper-only {(Cu^{II})$_n$−(O_2^{n-}), n = 1: 410 nm; n = 2: 525, 610 nm}[28,30,47] species involving **1a** or **1b**, respectively, despite the large UV−visible spectral differences observed. Definitive assignment of **3** as a mixed-metal μ-peroxo O_2-adduct was provided by rR spectroscopy, vide infra.

MALDI-TOF-MS of 3. MALDI-TOF mass spectrometry proved to be amenable to the study of **3** (Figure 2). In addition to the observation of **1a** {812 *m/z*, (M + H$^+$)$^+$} and **1b** {354 *m/z*, [M − (ClO_4^-)]$^+$}, oxygenation of the reduced complexes (F_8TPP)Fe^{II}/[(TMPA)Cu^{I}(MeCN)]$^+$ (**1a**/**1b** = 1:1) with $^{16}O_2$ resulted in the formation of a new peak (1239 *m/z*), corresponding to the molecular cation of complex **3** and a molecule of acetonitrile, [(F_8TPP)Fe^{III}−(O_2^{2-})−Cu^{II}-(TMPA)(MeCN)]$^+$. This peak shifted upon $^{18}O_2$ substitution to 1243 *m/z*, a shift of 4 amu, as expected for the $^{18}O_2$-adduct (i.e., peroxo complex) formulated. With the results of the rR,[21] Mossbauer (vide infra), and EXAFS[32] spectroscopic studies indicating a five-coordinate high-spin ferric heme (the fifth ligand being the bound peroxide), acetonitrile coordina-

(36) Wilson Jr., E. B.; Decius, J. C.; Cross, P. C. *Molecular Vibrations*; Dover Publications: New York, 1980.
(37) Woodward, L. A. *Introduction to the Theory of Molecular Vibrations and Vibrational Spectroscopy*; Claredon Press: Oxford, 1972.
(38) Miyazawa, T. *J. Chem. Phys.* **1958**, *29*, 246.
(39) Nelder, J. A.; Mead, R. *Comput. J.* **1965**, *7*, 308.
(40) Henson, M. J.; Vance, M. A.; Zhang, C. X.; Liang, H.-C.; Karlin, K. D.; Solomon, E. I. *J. Am. Chem. Soc.* **2003**, *125*, 5186−5192.
(41) Frisch, M. J.; Trucks, G. W.; Schlegel, H. B.; Scuseria, G. E.; Robb, M. A.; Cheeseman, J. R.; Montgomery, J. A., Jr.; Vreven, T.; Kudin, K. N.; Burant, J. C.; Millam, J. M.; Iyengar, S. S.; Tomasi, J.; Barone, V.; Mennucci, B.; Cossi, M.; Scalmani, G.; Rega, N.; Petersson, G. A.; Nakatsuji, H.; Hada, M.; Ehara, M.; Toyota, K.; Fukuda, R.; Hasegawa, J.; Ishida, M.; Nakajima, T.; Honda, Y.; Kitao, O.; Nakai, H.; Klene, M.; Li, X.; Knox, J. E.; Hratchian, H. P.; Cross, J. B.; Bakken, V.; Adamo, C.; Jaramillo, J.; Gomperts, R.; Stratmann, R. E.; Yazyev, O.; Austin, A. J.; Cammi, R.; Pomelli, C.; Ochterski, J. W.; Ayala, P. Y.; Morokuma, K.; Voth, G. A.; Salvador, P.; Dannenberg, J. J.; Zakrzewski, V. G.; Dapprich, S.; Daniels, A. D.; Strain, M. C.; Farkas, O.; Malick, D. K.; Rabuck, A. D.; Raghavachari, K.; Foresman, J. B.; Ortiz, J. V.; Cui, Q.; Baboul, A. G.; Clifford, S.; Cioslowski, J.; Stefanov, B. B.; Liu, G.; Liashenko, A.; Piskorz, P.; Komaromi, I.; Martin, R. L.; Fox, D. J.; Keith, T.; Al-Laham, M. A.; Peng, C. Y.; Nanayakkara, A.; Challacombe, M.; Gill, P. M. W.; Johnson, B.; Chen, W.; Wong, M. W.; Gonzalez, C.; Pople, J. A. *Gaussian 03*, revision C.02; Gaussian, Inc.: Wallingford, CT, 2004.
(42) Becke, A. D. *Phys. Rev. A* **1988**, *38*, 3098−3100.
(43) Perdew, J. P. *Phys. Rev. B* **1986**, *33*, 8822−8824.
(44) Portman, S.; Luth, H. P. *Chimia* **2000**, *54*, 766−770.
(45) See Supporting Information.
(46) Nanthakumar, A.; Fox, S.; Karlin, K. D. *J. Chem. Soc. Chem. Commun.* **1995**, 499−501.
(47) Karlin, K. D.; Wei, N.; Jung, B.; Kaderli, S.; Niklaus, P.; Zuberbühler, A. D. *J. Am Chem. Soc.* **1993**, *115*, 9506−9514.

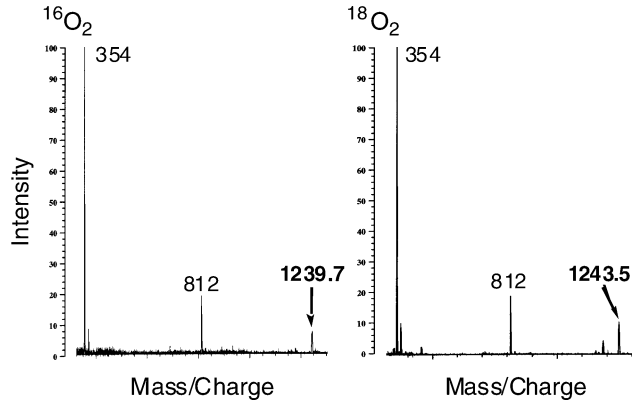

Figure 2. MALDI-TOF mass spectra of $[(F_8TPP)Fe^{III}-(O_2^{2-})-Cu^{II}(TMPA)]^+$ (**3**), formed from $^{16}O_2$ (left) and $^{18}O_2$ (right).

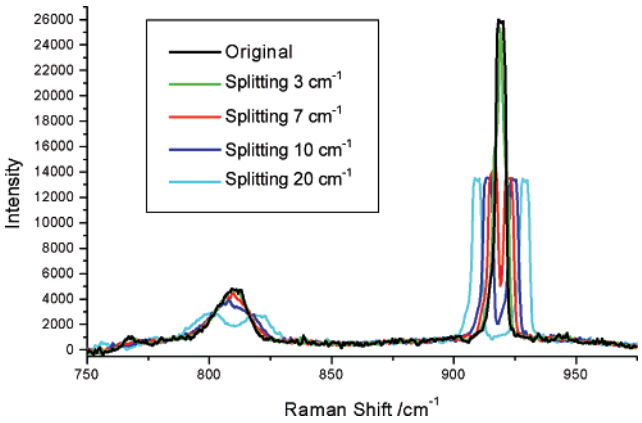

Figure 3. Resonance Raman spectra (black) of $[(F_8TPP)Fe^{III}-(O_2^{2-})-Cu^{II}(TMPA)]^+$ (**3**) in MeCN solution using 676-nm excitation at liquid nitrogen temperature. The calculated effect of splitting in the 810 cm^{-1} O−O stretch is compared with the 920 cm^{-1} solvent vibration.

tion to the heme is excluded. Further, the EXAFS study[32] of **3** does not support MeCN binding to the copper either, and we suggest that the increase in mass of the molecular cation observed (in mass spectrometry, vide supra) for **3** corresponds to the solution species plus one solvent molecule.

rR Spectroscopy of 3. The intermediate **3** was initially[21] characterized by rR spectroscopy (Figure S3)[45] using a 413-nm excitation coinciding with its Soret absorption maximum. Spectra from different dioxygen isotope labeling experiments were normalized with the intense phenyl vibrational mode at 898 cm^{-1}. An $^{16}O_2$ (Figure S3A) minus $^{18}O_2$ (Figure S3C) difference spectrum (Figure S3D)[45] singles out a unique isotope sensitive band at 808 cm^{-1}, downshifted by −46 cm^{-1} with $^{18}O_2$. To allow a definitive assignment of the 808 cm^{-1} feature to a peroxo ν(O−O) stretching vibration rather than a ferryl−oxo ν(Fe═O) mode, the experiments were repeated using mixed-isotope $^{16}O^{18}O$, derived from a 1:2:1 mixture of $^{16}O_2/^{16}O^{18}O/^{18}O_2$ (Figure S3B).[45] In addition to the positive signal at 808 cm^{-1} and its negative $^{18}O_2$-counterpart at 762 cm^{-1}, the isotopic mixture minus pure $^{16}O_2$ difference spectrum reveals a new signal at ∼785 cm^{-1}, assigned to $\nu(^{16}O-^{18}O)$ (Figure S3E).[45] The observation of this third signal excludes the ν(Fe═O) possibility, since only two stretching frequencies would be expected for a ferryl species. Porphyrin ligand vibrations consistent with the

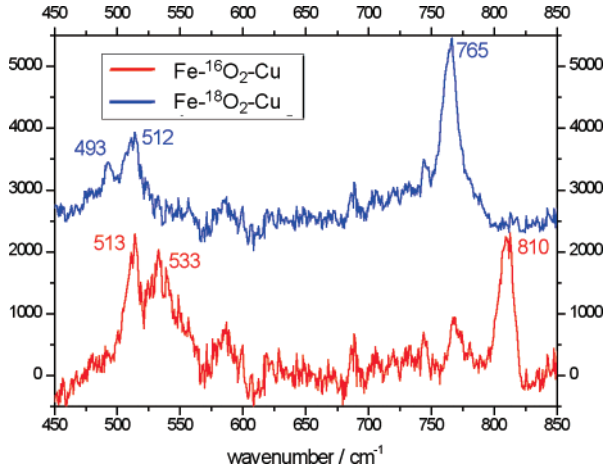

Figure 4. Resonance Raman spectra of $[(F_8TPP)Fe^{III}-(O_2^{2-})-Cu^{II}(TMPA)]^+$ (**3**), formed by oxygenation of $(F_8TPP)Fe^{II}/[(TMPA)-Cu^{I}(MeCN)]^+$ (**1a**/**1b** = 1:1) in MeCN at − 40 °C using $^{16}O_2$ (red) and $^{18}O_2$ gas (blue; offset by 2500 counts). All spectra were obtained at liquid nitrogen temperature with a 676-nm excitation in MeCN solvent.

presence of a five-coordinate high-spin ferric heme were observed, suggesting that **3** lacks a sixth axial base ligand.

The ν(O−O) of **3** {808 cm^{-1}; $\Delta^{16}O_2/^{18}O_2$ = 46 cm^{-1}; $\Delta^{16}O_2/^{16/18}O_2$ = 23 cm^{-1}} is in the range expected for a peroxide-level dioxygen adduct (Table 1). The possibilities of **3** being either the copper-only intermolecular peroxide adduct $[\{(TMPA)Cu^{II}\}_2-(O_2^{2-})]^{2+}$ [ν(O−O) = 832 cm^{-1} {$\Delta^{16}O_2/^{18}O_2$ = 44 cm^{-1}, EtCN}],[48] or a heme−peroxo−heme complex are ruled out by the rR and NMR data (vide infra), respectively. Additional relevant heme and/or Cu metal-bound peroxides with available vibrational data (Table 1) include (i) mononuclear anionic η^2-heme−peroxo complexes, $[(P)Fe^{III}-(O_2^{2-})]^-$, of Valentine and co-workers;[49,50] (ii) homobinuclear dicopper(II)−peroxo complexes (i.e., $[\{(L)-Cu^{II}\}_2-(O_2^{2-})]^{2+}$) of Karlin and co-workers for the copper chelates commonly used in heme−Cu complexes;[40,48,51,52] (iii) heterobinuclear heme−peroxo−Cu complexes, including **III**−**VI** (see Introduction).[20−26] Comparison of the vibrational data in Table 1 readily shows two significant traits for heme−peroxo−Cu complexes. First, the use of untethered ligands (as in **3**, **VI**) leads to O−O stretching frequencies ∼20 cm^{-1} higher than their tethered analogues (**IV**, **V**), suggesting that the geometric constraints (the details of which are not yet understood) imposed by binucleating ligands strains or distorts the peroxide's metal binding, whereas mononuclear components lead to $Fe^{III}-(O_2^{2-})-Cu^{II}$ cores which assume a more favorable geometry, leading to stronger O−O bonds. Second, the μ-η^2:η^1 binding mode (as in **3** (Scheme 1 and Introduction) and **III** (Chart 1)) exhibits a stronger O−O bond [ν(O−O) greater by ∼40 cm^{-1}] than for the μ-η^2:

(48) Baldwin, M. J.; Ross, P. K.; Pate, J. E.; Tyeklár, Z.; Karlin, K. D.; Solomon, E. I. *J. Am. Chem. Soc.* **1991**, *113*, 8671−8679.
(49) Selke, M.; Sisemore, M. F.; Valentine, J. S. *J. Am. Chem. Soc.* **1996**, *118*, 2008−2012.
(50) Burstyn, J. N.; Roe, J. A.; Miksztal, A. R.; Shaevitz, B. A.; Lang, G.; Valentine, J. S. *J. Am. Chem. Soc.* **1988**, *110*, 1382−1388.
(51) Liang, H.-C.; Karlin, K. D.; Dyson, R.; Kaderli, S.; Jung, B.; Zuberbühler, A. D. *Inorg. Chem.* **2000**, *39*, 5884−5894.
(52) Obias, H. V.; Lin, Y.; Murthy, N. N.; Pidcock, E.; Solomon, E. I.; Ralle, M.; Blackburn, N. J.; Neuhold, Y.-M.; Zuberbühler, A. D.; Karlin, K. D. *J. Am. Chem. Soc.* **1998**, *120*, 12960−12961.

Table 1. Resonance Raman Data for Various Peroxo-Level Dioxygen Adducts

complex	$\nu(^{16}O-^{16}O)$ ($-\Delta^{16}O_2/^{18}O_2$, $-\Delta^{16}O_2/^{16/18}O_2$), cm^{-1}	ref
[(F_8TPP)Fe^{III}−(O_2^{2-})−Cu^{II}(TMPA)]$^+$ (**3**)	808 (46, 23) μ-η^2:η^1	this work
[(TMP)Fe^{III}−(O_2^{2-})−Cu^{II}(5-MeTPA)]$^+$ (**III**)	790 (44) μ-η^2:η^1	26
[(^{6}L)Fe^{III}−(O_2^{2-})−Cu^{II}]$^+$ (**IV**)	788 (44, 21)	20,22
[(^{2}L)Fe^{III}−(O_2^{2-})−Cu^{II}]$^+$ (**V**)	747 (40, 17) μ-η^2:η^2	24
[(F_8TPP)Fe^{III}−(O_2^{2-})−Cu^{II}(L^{Me2N})]$^+$ (**VI**)	767 (41), 752 (45) μ-η^2:η^2	25
[(TPP)Fe^{III}−(O_2^{2-})−Cu^{II}(TPA)]$^+$	803 (44, 22)	53,54
[(TPP)Fe^{III}−(O_2^{2-})−Cu^{II}(5−MeTPA)]$^+$	793 (42)	53
[(DHIm)(a_3TACNaAcr)Fe^{III}−(O_2^{2-})−Cu^{II}]$^+$	758 (18)	55
[(OEP)Fe^{III}−(O_2^{2-})]$^-$	808 (47) η^2-peroxo	50
[(F_{20}TPP)Fe^{III}−(O_2^{2-})]$^-$	802 (n/a) η^2	49
[{(TMPA)Cu^{II}}$_2$−(O_2^{2-})]$^{2+}$	832 (44)	48
[{(L^{Me2N})Cu^{II}}$_2$−(O_2^{2-})]$^{2+}$	729 (40) μ-η^2:η^2	40
[{(MePY2)Cu^{II}}$_2$−(O_2^{2-})]$^{2+}$	730 (39), μ-η^2:η^2 588 (28), bis-μ-oxo core	52

Table 2. Experimental (Resonance Raman 676-nm Excitation), (NCA), and [DFT] Calculated Vibrational Frequencies (cm^{-1}) for the μ-η^2:η^1 Fe−O_2−Cu Core Structure

mode	^{16}O(1)−^{16}O(2)	^{18}O(1)−^{18}O(2)	^{16}O(1)−^{18}O(2)	^{18}O(1)−^{16}O(2)
ν(OO)	810	765	786	786
	(810)	(765)	(790)	(787)
	[885]	[832]	[853]	[853]
ν(Fe−O2)	533	513	[a]	[a]
	(536)	(509)	(520)	(531)
	[488]	[471]	[471]	[488]
ν(Fe−O1−Cu)$_a$	512	493	[a]	[a]
	(516)	(490)	(503)	(495)
	[429]	[422]	[429]	[422]
ν(Fe−O1−Cu)$_s$	(156)	(155)	(155)	(155)
	[110]	[108]	[108]	[109]

[a] A broad peak is observed centered at 511 cm^{-1}.

η^2 side-on peroxo geometry. As has been previously discussed in detail,[5,17,23−25] the origins of this difference appear to copper−ligand dependent: tetradentate copper chelates yield μ-η^2:η^1 dioxygen adducts, whereas tridentate ones lead to μ-η^2:η^2 O_2-binding. Further studies will be required to greater elucidate the interplay between structure, bonding, and vibrational properties of iron−peroxo−copper centers.

Absence of Splitting of the Mixed-Isotope Signal in 3. The absence of a splitting of the mixed-isotope signal at 785 cm^{-1} (vide supra) would be consistent with a symmetrically bound peroxide ligand (see diagram), in either a μ-1,2 (**A**, end-on) or μ-η^2:η^2 (**B**, side-on) geometry, and would seem

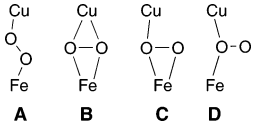

to rule out a μ-η^2:η^1 (**C**) or μ-1,1 bridging mode (**D**).

However, we have recently shown using a combination of both X-ray absorption spectroscopy (i.e., EXAFS) and DFT calculations that the bound peroxide in **3** assumes a μ-η^2:η^1 geometry (structure **C**, diagram) like that of Naruta's established (by X-ray) complex (**III**, Chart 1).[32] On the other hand, the predicted splitting-of-the-splitting of the O−O vibration (for ^{16}O−^{18}O) according to the DFT calculation and NCA (see below) is 1 and 3 cm^{-1}, respectively, which may not be spectroscopically (rR) observable.

Figure 3 shows the rR data obtained using a 676-nm excitation in the 750−1000 cm^{-1} region. The O−O stretch at 810 cm^{-1} and a solvent peak at 920 cm^{-1} are observed in this region. In order to determine the minimum splitting that could be observed for the O−O stretch under experimental conditions, we simulated the effect of splitting the energy position of these peaks by increasing cm^{-1}. Split spectra were generated from the experimental $^{16}O_2$ spectrum (with noise) in three steps: (i) two new spectra were created from the $^{16}O_2$ peak that were shifted to higher and lower energy by equal wavenumbers; (ii) the new shifted spectra were added and renormalized to the original intensity; (iii) this "split" spectrum was overlaid with the original, experimental data to see if there were differences in shape resolvable over the noise level. In the case of the sharp solvent peak at 920 cm^{-1}, an effect on the vibrational band shape of the signal is apparent for a 3 cm^{-1} splitting and two distinctive peaks are observed for 7 cm^{-1} (Figure S4).

However, the O−O stretch at 810 cm^{-1} is significantly broader. The effect of energy splitting on the shape of the signal is only apparent above 10 cm^{-1}, and two distinctive peaks are only observed for a 20 cm^{-1} spectrum (Figure S5). Therefore, a μ-η^2:η^1 bonding mode for the peroxide moiety in **3** cannot be ruled out on the basis of the lack of splitting of the 785 cm^{-1} O−O stretch of the mixed-isotope experiment (Figure S3)[45] since the predicted splitting (<3 cm^{-1} according to NCA and DFT) is too small to be observed for such a broad vibration under the experimental conditions.

Presence of Two M−O Stretching Frequencies in 3. In order to obtain further insight into its structure, complex **3** was also characterized by rR spectroscopy using a 676-nm excitation. Under these experimental conditions, the porphyrin Raman peaks are not resonance enhanced and the O−O vibration (at 810 cm^{-1}) and two different M−O vibrations at (533 and 511 cm^{-1}) are easily observed (see Figure 4 and Table 2). All three bands are $^{18}O_2$ isotope sensitive, with the 810 cm^{-1} band shifting down by 45 cm^{-1}, while the bands at 533 and 511 cm^{-1} are shifted down in energy by −20 and −19 cm^{-1}, respectively, allowing their assignment as M−O modes. The difference in intensity between the ^{16}O and ^{18}O sample is clearly observed using other excitation lines and it could be related to sample differences due to different methods of preparation. As an example, data using 775-nm excitation are included in Figure S6. Further insights derive from NCA, see below.

Table 3. Experimental and Calculated Vibrational Frequencies (cm^{-1}), Potential Energy Distribution (%, for the $^{16}O_2$ Isotopomer), and Selected Force Constants (mdyn/Å) from the NCA of the μ-η^2:η^1 Fe−O_2−Cu Core Structure[a]

	potential energy distribution			
mode	Δr(O−O)	Δr(Fe−O2)	Δr(Fe−O1)	Δr(Cu−O1)
ν(O−O)	80	6	8	5
ν(Fe−O2)	1	75	10	14
ν(Fe−O1−Cu)$_a$	20	15	33	32
ν(Fe−O1−Cu)$_s$	2	1	49	48
force constants	κ(O−O)	κ(Fe−O2)	κ(Cu−O1)	κ(Fe−O1)
	2.66	2.49	1.43	1.50

[a] O1 bridges both Fe and Cu, while O2 is only iron-bound.

NCA in 3. To obtain a quantitative description of the observed vibrational modes, 810, 533, and 513 cm^{-1}, a NCA was performed using the *xyz* coordinates of the μ-η^2:η^1 Fe−O_2−Cu core structure derived from our published DFT calculations.[32] Only in-plane vibrations were included, and a generalized force field was used. The O−O stretch, the three possible nonequivalent M−O stretches, and their interaction constants were floated to fit the experimental vibrational frequencies and their isotopes shifts. The calculated vibrational frequencies are presented in Table 2. Force constants, normal mode eigenvectors, and potential energy distribution are summarized in Table 3, while the resulting atom-displacement matrix is given as Supporting Information (Table S1 and Figure S7).[45]

The calculated frequencies and isotope shifts are consistent with the experimental data. The calculated PEDs and normal mode eigenvectors indicate that the 810 cm^{-1} mode is indeed a dominant ν(O−O) vibration (80% O−O + 8% Fe−O1 + 6% Fe−O2 + 4% Cu−O1, where O1 is the oxygen atom that is bound to both the copper and iron; O2 is the oxygen atom that is only bound to the iron). The 533 cm^{-1} mode corresponds mainly to the ν(Fe-O2) vibration (75% Fe−O2 + 14% Cu−O1 + 10% Fe−O1 + 1% O−O), while the 513 cm^{-1} mode can be assigned to an asymmetric Fe−O1−Cu vibration (33% Fe−O1 + 32% Cu−O1 + 20% O−O + 14% Fe−O2). NCA predicts the presence of a low-energy mode at 156 cm^{-1} that can be assigned to the symmetric Fe−O1−Cu stretch (49% Fe−O1 + 48% Cu−O1 + 2% O−O + 1% Fe−O2). Our attempts to locate such low-energy bands experimentally have been unsuccessful, as this energy region is obscured by vibrations from the solvent (MeCN). Attempts to locate this low-energy absorption using a solid sample of **3** were also unsuccessful. However, the DFT frequencies calculated for the model complex [(P)Fe^{III}−(O_2^{2-})−Cu^{II}(TMPA)]$^+$ are in agreement with the results from the NCA analysis showing a symmetric Fe−O1−Cu stretch at 110 cm^{-1}. In summary, the rR spectra and NCA support the presence of a μ-η^2:η^1 peroxide ligand in complex **3**.

^{2}H NMR Spectroscopy of 3. By selectively deuterating the pyrrole hydrogens, a full ^{2}H NMR spectroscopic investigation was performed to complement the previously reported ^{1}H NMR study[21] and provided unambiguous assignment of the pyrrole hydrogens. Such assignments are possible due to the wealth of information available pertaining to heme oxidation and spin state as deduced from pyrrole resonance assignments[56−58] and from an independent NMR spectroscopic study carried out on the dioxygen reactivity of **1a**.[27]

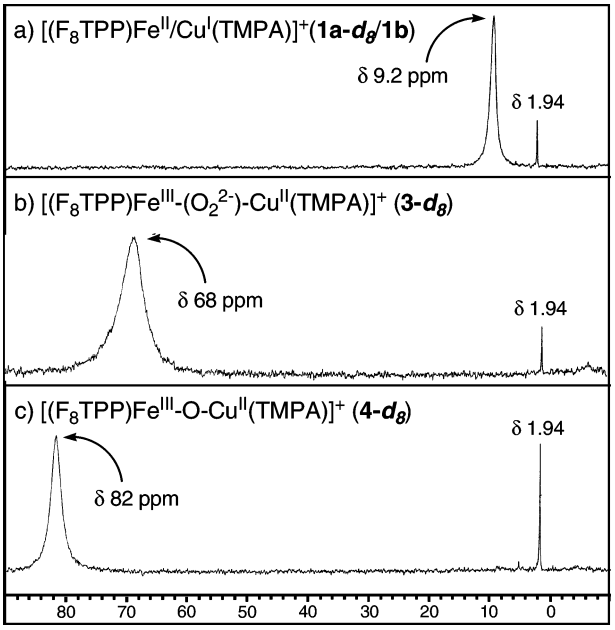

Figure 5. ^{2}H NMR spectra (MeCN, 233 K) of (F_8TPP-d_8)Fe^{II}/[(TMPA)-Cu^I(MeCN)]$^+$ (**1a-d_8/1b**) (a), [(F_8TPP-d_8)Fe^{III}−(O_2^{2-})−Cu^{II}(TMPA)](ClO_4) (**3-d_8**) (b), and [(F_8TPP-d_8)Fe^{III}−O−Cu^{II}(TMPA)]$^+$ (**4-d_8**) (c). The signal at δ 1.94 is due to the natural abundance of deuterium in the MeCN solvent.

The ^{2}H NMR spectra of the oxygenation reaction of the 1:1 mixture of (F_8TPP)Fe^{II} and [(TMPA)Cu^I(MeCN)]$^+$ (**1a**/**1b**) in MeCN at − 40 °C is shown in Figure 5. Prior to addition of dioxygen, the reduced complexes **1a/1b** exhibit a pyrrole resonance at δ 9.2 (Figure 5a), indicative of a low-spin ($S = 0$) six-coordinate (bis-MeCN) ferrous heme at low temperature, and supported by the Evans method magnetic moment measurement {$\mu_B = 0$; no paramagnetically shifted solvent peak was observed downfield from the reference/capillary solvent resonance}. Direct injection of O_2 into the chilled NMR tube leads to the formation of **3**, with a downfield shifting of the pyrrole resonance to δ 68 (Figure 5b), indicative of a high-spin ferric heme[56−58] (and supported by the rR study, vide supra). We have also noted in the ^{1}H NMR study of **3** that upfield-shifted peaks were also seen at δ −11 and −20. We have reported this characteristic pattern of downfield-shifted pyrrole resonances and upfield shifted peaks in similar (P)Fe^{III}−X−Cu^{II} (X = O_2^{2-}, O^{2-}) systems

(53) Naruta, Y.; Sasaki, T.; Tani, F.; Tachi, Y.; Kawato, N.; Nakamura, N. *J. Inorg. Biochem.* **2001**, *83*, 239−246.
(54) Sasaki, T.; Nakamura, N.; Naruta, Y. *Chem. Lett.* **1998**, 351−352.
(55) Collman, J. P.; Herrmann, P. C.; Boitrel, B.; Zhang, X.; Eberspacher, T. A.; Fu, L.; Wang, J.; Rousseau, D. L.; Williams, E. R. *J. Am. Chem. Soc.* **1994**, *116*, 9783−9784.
(56) Goff, H. M. The Porphyrins (Goff review article). In *Iron Porphyrins*; Lever, A. B. P., Gray, H. B., Eds.; Addison-Wesley: Reading, MA, 1983; Part 1; pp 239−281.
(57) Walker, F. A.; Simonis, U. Proton NMR Spectroscopy of Model Hemes. In *Biological Magnetic Resonance*; Berliner, L. J., Reuben, J., Eds.; Plenum Press: New York, 1993; Vol. 12/NMR of Paramagnetic Molecules, pp 133−274.
(58) Walker, F. A. *Porphyrin Handbook* **2000**, *5*, 81−183.

Table 4. ^{19}F NMR Chemical Shifts of Heme and Heme−Cu Dioxygen Adducts

complex	δ_F (ppm)	solvent	temp, K
(F$_8$TPP)Fe^{II}/[(TMPA)Cu^{I}(MeCN)]$^+$ (**1a**/**1b**)	−113	CD_3CN	233
[(F$_8$TPP)Fe^{III}−(O$_2^{2-}$)−Cu^{II}(TMPA)]$^+$ (**3**)	−92	CD_3CN	233
[(F$_8$TPP)Fe^{III}−O-Cu^{II}(TMPA)]$^+$ (**4**)	−94, −98	CD_3CN	233
(F$_8$TPP)Fe^{II} (**1a**) [27]	−116	THF-d_8	193
	−107	CD_2Cl_2	193
(S)(F$_8$TPP)Fe^{III}−(O$_2^-$) [27] (iron−superoxo)	−111, −113	THF-d_8	193
[(F$_8$TPP)Fe^{III}]$_2$−(O$_2^{2-}$) [27] (Fe−peroxo−Fe)	−106, −109	CD_2Cl_2	193
(F$_8$TPP)Fe^{III}−OH [27] (iron−hydroxide)	−83	THF-d_8	193
	−79	CD_2Cl_2	193
[(F$_8$TPP)Fe^{III}]$_2$−O [62] (Fe−oxo−Fe)	−103, −109	CD_2Cl_2	RT

having $S = 2$ spin states,[20−23,59,60] including **4** {$\mu_B = 5.1 \pm 0.2$, Evans method, MeCN, −40 °C},[59] with previously assigned downfield-shifted pyrrole resonances (δ 83), and upfield-shifted TMPA-chelate peaks at δ −11 (pyridyl 5-H) and −28 (pyridyl 3-H) (Figure 5c).[59,60] The $S = 2$ spin state arises from the antiferromagnetic coupling of the $S = 5/2$ heme center to an $S = 1/2$ copper(II) moiety, through the bridging peroxo (in **3**) or oxo ligand (in **4**). Supporting an overall $S = 2$ spin state for **3** is the magnetic susceptibility measurement ($\mu_B = 5.1 \pm 0.2$; Evans method, MeCN, −40 °C), in close agreement with the spin-only value of 4.9 μ_B for four unpaired electrons. Ligand and/or spin-state dynamics might account for the broadness of the pyrrole resonance in **3**, although Mössbauer spectroscopic data (vide infra) do not give any hint of this possibility. The analogous tethered complex, **IV**, exhibits Curie−Weiss behavior (linear) in the limited temperature range of 228−288 K.[20]

Our independent ^{2}H NMR characterization of the dioxygen adducts of pyrrole-deuterated **1a**-d_8 excludes the possibility that the resonances observed for **3** might be derived from a mononuclear heme-superoxo complex, PFe^{III}−(O$_2^-$) {$\delta_{pyrrole} = \sim 7-10$ ppm},[27] or a heme−peroxo−heme binuclear complex, PFe^{III}−(O$_2^{2-}$)−Fe^{III}P {$\delta_{pyrrole} = \sim 15-19$ ppm}.[27,61]

^{19}F NMR Spectroscopy of 3. We have previously undertaken a ^{19}F NMR spectroscopic study of the heme-only **1a** oxygenation reaction, forming heme−superoxo, **2a**, and heme−peroxo−heme, [(F$_8$TPP)Fe^{III}]$_2$−(O$_2^{2-}$), dioxygen adducts.[27] The results of this study indicated that both the diamagnetic ($S = 0$) heme−superoxo complex and the antiferromagnetically coupled heme−peroxo−heme O$_2$-adduct have sharp fluorine resonances between δ −109 and −113 (Table 4). The mixture of the reduced complexes **1a**/**1b** also shows a single sharp fluorine resonance {Figure 6a: $\delta_F = -113$ ppm}, implying a symmetric environment for the eight fluorine substituents. These findings are in contrast to those observed for **3**, which exhibits a single (broad) fluorine resonance for the $S = 2$ heme−peroxo−Cu complex at δ −92 (Figure 6b). Additionally, **4** also gives rise to broad

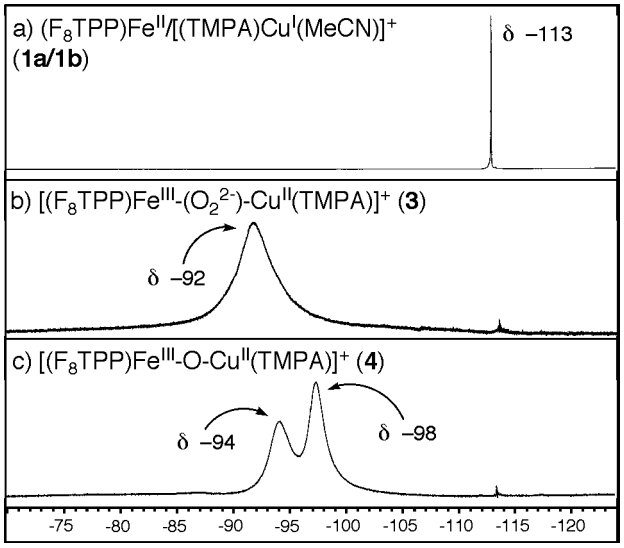

Figure 6. ^{19}F NMR spectra (CD_3CN, 233 K) of (F$_8$TPP)Fe^{II}/[(TMPA)-Cu^{I}(MeCN)]$^+$ (**1a**/**1b**) {$\delta_F = -113$ ppm} (a), [(F$_8$TPP)Fe^{III}−(O$_2^{2-}$)−Cu^{II}-(TMPA)](ClO$_4$) (**3**) {$\delta_F = -92$ ppm} (b), and [(F$_8$TPP)Fe^{III}−O−Cu^{II}-(TMPA)]$^+$ (**4**) {$\delta_F = -94, -98$ ppm} (c).

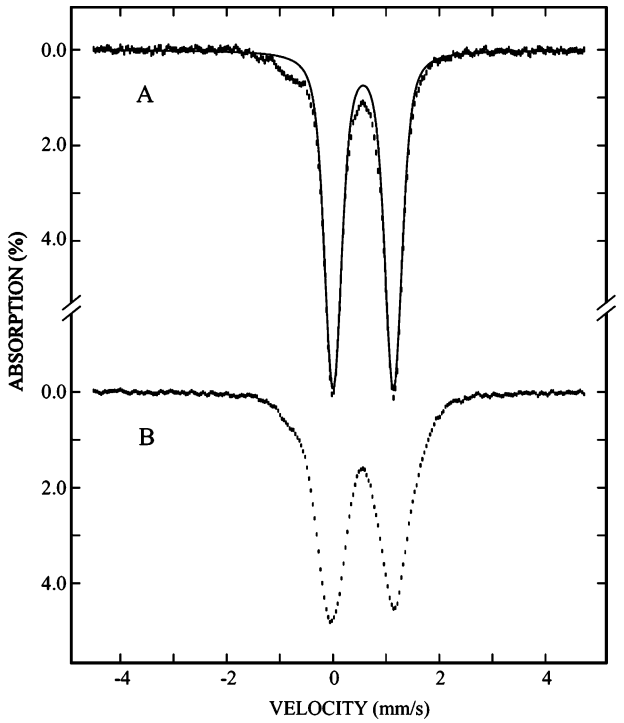

Figure 7. Mössbauer spectra of ^{57}Fe-labeled [(F$_8$TPP)Fe^{III}−(O$_2^{2-}$)−Cu^{II}-(TMPA)]$^+$ (**3**). The spectra (hashed marks) were recorded at 4.2 K in zero field (A), and in a field of 50 mT applied parallel to the γ-beam (B). The solid line in A is the simulation of a quadrupole doublet with $\Delta E_Q = 1.14$ mm/s, $\delta = 0.57$ mm/s.

fluorine resonances (Figure 6c: δ −94 and −98). The asymmetry of complex **4** can rationalize the differences in the fluorine environment of the 2,6-difluorophenyl substituents, leading to these two observed fluorine signals: one resonance accounts for the fluorines on the 'proximal' μ-oxo ligand side of the porphyrin macrocycle, the second resonance being attributed to those fluorines on the 'distal' side. However, the lack of asymmetry in **3** when compared to **4** is not readily apparent, and we speculate that either (i) the differences in the structure of **3** versus **4** give rise to the

(59) Nanthakumar, A.; Fox, S.; Murthy, N. N.; Karlin, K. D. *J. Am. Chem. Soc.* **1997**, *119*, 3898−3906.
(60) Kim, E.; Kamaraj, K.; Galliker, B.; Rubie, N. D.; Moënne-Loccoz, P.; Kaderli, S.; Zuberbühler, A. D.; Karlin, K. D. *Inorg. Chem.* **2005**, *44*, 1238−1247.
(61) Balch, A. L. *Inorg. Chim. Acta* **1992**, *198*−*200*, 297−307.

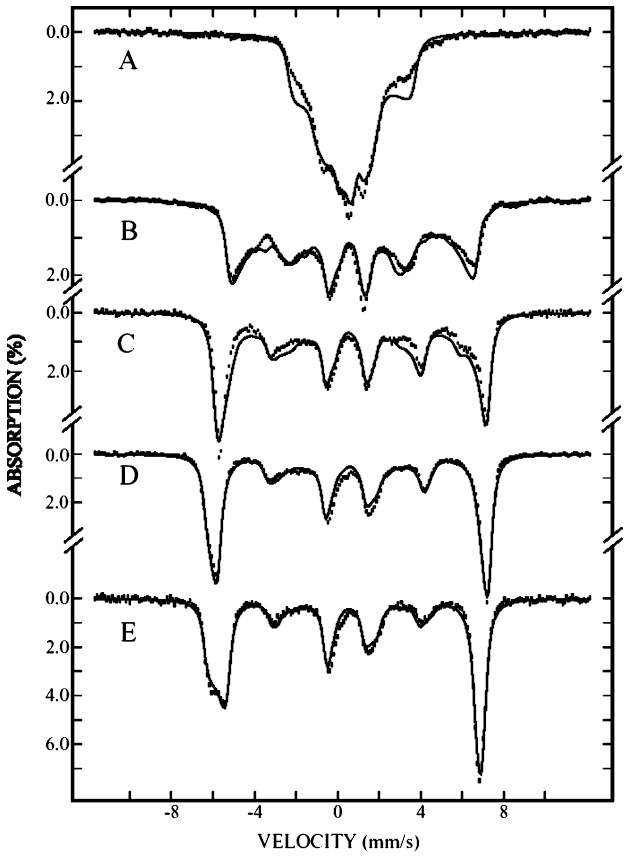

Figure 8. Field-dependent Mössbauer spectra of ^{57}Fe-labeled [(F_8TPP)-Fe^{III}−(O_2^{2-})−Cu^{II}(TMPA)]$^+$ (**3**). The spectra (hashed marks) were recorded at 4.2 K in a field of 0.25 (A), 1 (B), 2 (C), 4 (D), or 8 T (E) applied parallel to the γ-beam. The solid lines are theoretical simulations using the parameters listed in Table 5.

observed differences in fluorine resonance signals, with the μ-peroxo bridged complex having a somewhat more equivalent environment for the fluorine substituents (one signal), and the μ-oxo bridged system possessing more fluorine-environment inequivalency (hence, two signals), or (ii) ligand and/or spin-state dynamics lead to a single (albeit broad) observed peak in the limited observable temperature range where **3** is stable. For both the peroxo- and oxo-bridged complexes, we suggest that their $S = 2$ spin state leads to a broadening and downfield-shifting of the fluorine resonances to the region of δ −92 to −98, which is at least 10 ppm more downfield than the corresponding diamagnetic heme-only superoxo (**2a**) or peroxo complexes, and closer to the ^{19}F NMR chemical shift of the ferric-hydroxy ($S = 5/2$) (F_8TPP)Fe^{III}−OH complex (δ_F = −79 to −82 ppm).[27] The ^{19}F NMR spectra observed appear to be quite sensitive to the oxidation and spin states of the complexes studied and may in the future be utilized as an additional tool for gaining insight into the electronic nature of such heme-containing systems.

Mössbauer Spectroscopy of 3. ^{57}Fe-labeled **1a** was synthesized (see Experimental Section) and used in the oxygenation reaction with **1b** to form **3** (MeCN, 233 K) for further characterization by Mössbauer spectroscopy. The Mössbauer spectrum of **3** recorded at 4.2 K and in zero-field (Figure 7A) exhibits a sharp quadrupole doublet with parameters ($\Delta E_Q = 1.14$ mm/s and $\delta = 0.57$ mm/s) that are indicative of high-spin ferric compounds. The fact that the isomer shift of **3** is at the high end of the range of values (0.3−0.7 mm/s) observed for high-spin ferric compounds and is significantly larger than those (0.33−0.45 mm/s) observed specifically for high-spin ferric hemes[63] is consistent with binding of an electron-rich peroxide ligand to the Fe center.[50] Similarly large values (0.60−0.66 mm/s) of isomer shift have been observed for a few peroxide-bound high-spin ferric compounds, including Naruta's structurally characterized heme−peroxo−copper analogue (**III**, Chart 1; $\Delta E_Q = 1.17$ mm/s and $\delta = 0.56$ mm/s (77 K)),[26] an η^2-peroxo−iron(III)−porphyrinate,[50] and several non-heme peroxodiferric intermediates found in methane monooxygenase,[64,65] variants of the R2 subunit of *E. coli* ribonucleotide reductase,[66] stearoyl-acyl carrier protein desaturase,[67] and ferritin.[68] When a spectrum of **3** is recorded at 4.2 K in a weak applied field of 50 mT, the quadrupole doublet becomes significantly broadened (Figure 7B). This broadening is a consequence of magnetic hyperfine interaction (albeit small), the presence of which indicates that **3** is paramagnetic. The observation that a weak applied field induces only a small magnetic hyperfine interaction in **3** indicates further that **3** has an integer-spin ground state (vide infra), in accordance with the conclusion made from the NMR and susceptibility measurements that the $S = 5/2$ Fe^{III} heme and the $S = 1/2$ Cu^{II} site are spin coupled.

In order to gain further insight into the electronic state of **3**, Mössbauer spectra in various magnetic fields were recorded. Figure 8 shows the Mössbauer spectra of **3** recorded at 4.2 K in a field of 0.25 (A), 1 (B), 2 (C), 4 (D), or 8 T (E) applied parallel to the γ-beam. The overall splitting of the spectra, which is a measure of the strength of the magnetic hyperfine interaction, increases gradually with the applied field and reaches its full splitting at about 4 T. This observed field dependence is typical of integer spin systems[69] and is distinct from that of half-integer spin systems, of which the spectra exhibit full magnetic splitting at weak applied fields (for example, 50 mT). These field-dependent Mössbauer spectra of **3** were analyzed using the following spin Hamiltonian,

(62) Nanthakumar, A.; Goff, H. M. *Inorg. Chem.* **1991**, *30*, 4460−4464.
(63) Debrunner, P. G. In *Iron Porphyrins*; Lever, A. B. P., Gray, H. B., Eds.; VCH: New York 1990; pp 139−234.
(64) Liu, K. E.; Valentine, A. M.; Wang, D. L.; Huynh, B. H.; Edmondson, D. E.; Salifoglou, A.; Lippard, S. J. *J. Am. Chem. Soc.* **1995**, *117*, 10174−10185.
(65) Liu, K. E.; Wang, D. L.; Huynh, B. H.; Edmondson, D. E.; Salifoglou, a.; Lippard, S. J. *J. Am. Chem. Soc.* **1994**, *116*, 7465−7466.
(66) Bollinger, J. M.; Krebs, C.; Vicol, A.; Chen, S. X.; Ley, B. A.; Edmondson, D. E.; Huynh, B. H. *J. Am. Chem. Soc.* **1998**, *120*, 1094−1095.
(67) Broadwater, J. A.; Achim, C.; Munck, E.; Fox, B. G. *Biochemistry* **1999**, *38*, 12197−12204.
(68) Pereira, a. S.; Small, W.; Krebs, C.; Tavares, P.; Edmondson, D. E.; Theil, E. C.; Huynh, B. H. *Biochemistry* **1998**, *37*, 9871−9876.
(69) Surerus, K. K.; Hendrich, M. P.; Christie, P. D.; Rottgardt, D.; Orme-Johnson, W. H.; Munck, E. *J. Am. Chem. Soc.* **1992**, *114*, 8579−8590.

$$H = H_e + H_{hf} \quad (1)$$

where

$$H_e = D\left[S_z^2 - \frac{S(S+1)}{3} + \frac{E}{D}(S_x^2 - S_y^2)\right] + \beta \mathbf{S}\cdot\mathbf{g}\cdot\mathrm{H} \quad (2)$$

and

$$H_{hf} = \frac{eQV_{zz}}{4}\left[I_z^2 - \frac{I(I+1)}{3} + \frac{\eta}{3}(I_x^2 - I_y^2)\right] + (\langle \mathbf{S}\rangle\cdot\mathbf{A}\cdot\mathbf{I} - g_n\beta_n\mathbf{H}\cdot\mathrm{I}) \quad (3)$$

The Hamiltonian H_e represents the zero-field splitting terms (the first three terms in eq 2) and the electronic Zeeman interaction term ($\beta\mathbf{S}\cdot\mathbf{g}\cdot\mathbf{H}$) of the total electronic spin of the ground state, $S = 2$, and H_{hf} represents the electronic nuclear hyperfine interactions, which include the quadrupole interaction (the first three terms in eq 3), the magnetic hyperfine interaction between the electronic spin, **S**, and the ^{57}Fe nuclear spin, **I** ($\langle \mathbf{S}\rangle\cdot\mathbf{A}\cdot\mathbf{I}$), and the nuclear Zeeman interaction ($g_n\beta_n\mathbf{H}\cdot\mathbf{I}$). On the basis of the NMR and susceptibility results, a system spin $S = 2$ was used for the analysis of the Mössbauer spectra of **3**. As Mössbauer absorptions are arising from ^{57}Fe nuclear transitions, the spectra are basically determined by H_{hf} of eq 3. For a paramagnetic system, the magnetic hyperfine interaction $\langle \mathbf{S}\rangle\cdot\mathbf{A}\cdot\mathbf{I}$ is generally the dominating term in H_{hf} and, thus, has a decisive effect on the observed Mössbauer spectra. For high-spin ferric hemes, the magnetic hyperfine tensor, $\mathbf{A}_{heme}$, is rather isotropic and varies within a narrow range (−21 to −18 T).[63] For a spin-coupled system, such as **3**, the apparent **A** tensor of the system is related to the intrinsic **A** tensor, such as $\mathbf{A}_{heme}$, by a simple factor depending on the nature of the spin coupling.[70] Consequently, the acceptable values for **A** in eq 3 are restricted within a limited range. The spectra therefore depend strongly on the spin expectation value, $\langle \mathbf{S}\rangle$, which in turn is determined by the zero-field splitting parameters D and E/D and the applied magnetic field, **H**. In other words, the parameters D and E/D can be determined accurately from the analysis of the field-dependent spectra of **3**. A global analysis including all the spectra recorded at 4.2 K in various applied fields (0−8 T) yielded the spin Hamiltonian parameters for **3** (Table 5). Simulations using these parameters are plotted as solid lines overlaid with the experimental data in Figure 8. The intrinsic values for the zero-field splitting parameter and the magnetic hyperfine tensor of the high-spin ferric heme (D_{heme} and $\mathbf{A}_{heme}$, respectively) can be obtained from the values of the corresponding parameters determined for the spin-coupled system by standard spin projection techniques,[70]

$$D_{heme} = (3/4)D = 2.2\ \mathrm{cm}^{-1}$$

and

$$\mathbf{A}_{heme}/g_n\beta_n = (6/7)(\mathbf{A}/g_n\beta_n) = (-22.0, -19.6, -18.0)\ \mathrm{T}$$

(70) Bencini, A.; Gatteschi, D. *Electron Paramagentic Resonance of Exchange Coupled Systems*; Springer-Verlag: Berlin, 1990.

Table 5. Mössbauer Spectroscopic Parameters for [(F$_8$TPP)^{57}Fe^{III}−(O$_2^{2-}$)−Cu^{II}(TMPA)]$^+$ (**3**) and [(F$_8$TPP)^{57}Fe^{III}−O−Cu^{II}(TMPA)]$^+$ (**4**)

complex	**3**	**4**
D^a (cm^{-1})	2.9	5.6
E/D	0.15	0.01
δ (mm/s)	0.57	0.48
ΔE_Q (mm/s)	−1.14	−1.17
η	0.35	0
α^b (°)	25	0
β^b (°)	59	0
γ^b (°)	118	0
$A_{xx}/g_n\beta_n$ (T)	−25.7	−23.7
$A_{yy}/g_n\beta_n$ (T)	−22.9	−23.7
$A_{zz}/g_n\beta_n$ (T)	−21.0	−23.7

[a] Calculated for an $S = 2$ spin system. [b] Euler angles rotating the principal axis frame of the electric field gradient tensor into that of the zero-field splitting tensor.

The magnitude and small anisotropy observed for $\mathbf{A}_{heme}$ are consistent with the high-spin ferric assignment. The zero-field splitting parameter, $D_{heme} = 2.2\ \mathrm{cm}^{-1}$, determined for **3**, however, is significantly smaller than those (4−22 cm^{-1}) observed for high-spin ferric heme compounds. It is therefore worthy of note that one other heme compound that was reported to have an unusually small D of 0.85 cm^{-1} is also a peroxide-bound high-spin ferric heme, [(OEP)Fe^{III}O$_2^{2-}$]$^-$ [$E/D = 0.29$].[50] The rhombicity parameter, $E/D = 0.15$, determined for **3** is also unusual for heme compounds, which are axially symmetric and generally exhibit an E/D value of about 0.02. In this respect, it is interesting to compare the E/D value of **3** with that of the decay product, **4**. We have recorded the spectra of **4** in MeCN at 4.2 K in various applied fields ranging from 0 to 8 T (Figure S8). Analysis of these data using eqs 1−3 yielded the parameters listed in Table 5. These parameters are very similar to those published earlier for the crystalline form of **4**[31] and for a similar oxo-bridged heme−Cu complex, [(OEP)Fe−O−Cu(Me$_6$-tren)]$^+$.[71] The E/D value of 0.03 determined for **4** is normal for heme compounds and can be understood as a consequence of the linear Fe−O−Cu bridge, for which the π-donor interactions between the Fe and O along the heme normal (d_{xz}(Fe)−p_x-(O) and d_{yz}(Fe)−p_y(O)) are expected to be similar. The large rhombicity observed for complex **3** may thus suggest a side-on or bent end-on Fe−peroxide binding mode, with the side-on geometry consistent with the results of the EXAFS spectroscopic and DFT structural studies of **3**.[32]

Kinetics of the 1a/1b Oxygenation Reaction. The oxygenation reaction of **1a**/**1b** was performed in propionitrile[72] due to the known previously investigated kinetics and thermodynamics of formation of the resulting dioxygen adducts of the individual mononuclear iron[27] and copper[30,73] components. At −90 °C, addition of O$_2$ to **1a**/**1b** resulted in

(71) Kauffmann, K. E.; Goddard, C. A.; Zang, Y.; Holm, R. H.; Münck, E. *Inorg. Chem.* **1997**, *36*, 985−993.

(72) In the text, the tmpa−Cu(I) complex is always associated with MeCN, e.g., as [(TMPA)Cu^I(MeCN)]$^+$ (**1b**), since it is synthesized in and isolated from MeCN. Descriptions of solution chemistry in propionitrile solvent thus obviously deal with the chemistry of [(TMPA)-Cu^I(EtCN)]$^+$, including in the kinetics investigations carried out in EtCN, cf. Scheme 2.

(73) Zhang, C. X.; Kaderli, S.; Costas, M.; Kim, E.-i.; Neuhold, Y.-M.; Karlin, K. D.; Zuberbühler, A. D. *Inorg. Chem.* **2003**, *42*, 1807−1824.

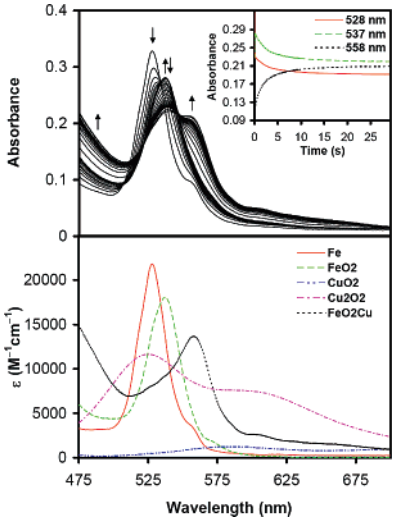

Figure 9. Top: Time-dependent oxygenation of $(F_8TPP)Fe^{II}$/[(TMPA)-Cu^{I}(MeCN)]$^+$ (**1a**/**1b**); $[(F_8TPP)Fe^{II}] = 8.463 \times 10^{-5}$ M, [{(TMPA)Cu^{I}-(MeCN)}$^+$] $= 8.469 \times 10^{-5}$ M ,$[O_2] = 5.02 \times 10^{-3}$ M in EtCN {183 K, $t_{total} = 30$ s}.[72] Inset: $\lambda = 528$ nm (red), decay of $(F_8TPP)Fe^{II}$; $\lambda = 558$ nm (black), formation of $[(F_8TPP)Fe^{III}-(O_2^{2-})-Cu^{II}(TMPA)]^+$ (**3**); $\lambda =$ 537 nm (green), formation and decay of $(EtCN)(F_8TPP)Fe^{III}-(O_2^-)$ (**2a**). Bottom: Calculated spectra for species in the **1a**/**1b**/O_2 reaction, following kinetics analysis for determination of k_4. All other rate constants (Scheme 2) and spectra of Cu-only species were fixed at published values (see text).

decay of the 528 nm band (reduced **1a**) and formation of a transient species ($\lambda_{max} = 537$ nm) within the first ~30 ms (Figures 9 and S9).[45] The spectral features and kinetic behavior for the formation of this intermediate matched those previously observed for the **1a**/O_2 reaction in EtCN despite the presence of **1b**, establishing this 537 nm species as the mononuclear low-spin heme−superoxo intermediate **2a** ($\nu_{O-O} = 1178$ cm^{-1}, $\nu_{Fe-O} = 568$ cm^{-1}, in tetrahydrofuran solvent).[21,25] Additional support for this conclusion is provided by Mössbauer spectroscopy (vide infra).

While our spectroscopic monitoring (500−700 nm) was unable to confirm or deny the presence of a copper(II)−superoxide intermediate (because of the dominance of intense heme absorptions), our previous stopped-flow kinetic studies[29,73] of the oxygenation reaction of only **1b** in EtCN[72] confirm its presence {**2b**, $\lambda_{max} = 410$ nm}, formed on the millisecond time scale, prior to its eventual combination with **1b** to give the end-on-bound μ-1,2-peroxo complex [{(TMPA)-Cu^{II}}$_2$−(O_2^{2-})]$^{2+}$ {$\lambda_{max} = 525$ nm}. Thus, it is concluded that both **1a** and **1b** undergo simultaneous and independent reversible oxygenation reactions even when mixed together as in the present system, Scheme 2 (k_1/k_{-1}, k_2/k_{-2}, and k_3/k_{-3} processes).

Decay of the heme−superoxo intermediate **2a** occurred over the next 20−25 s (Figures 9 and S9),[45] with formation of a $\lambda_{max} = 558$ nm species, consistent with **3** (Figure 9). Kinetic analysis of this 537 → 558 nm transformation, corresponding to the reaction of **2a** with **1b** to give **3**, was fit to the model described in Scheme 2, where all rate constants except k_4 were fixed according to their known values from independent measurements in EtCN.[25,27,29,73] This approach simplified the system leading to the determination of the rate constant k_4 (see Eyring plot for k_4, Figure S10).[45] The results are given in Table 6. Overall, the activation

Scheme 2

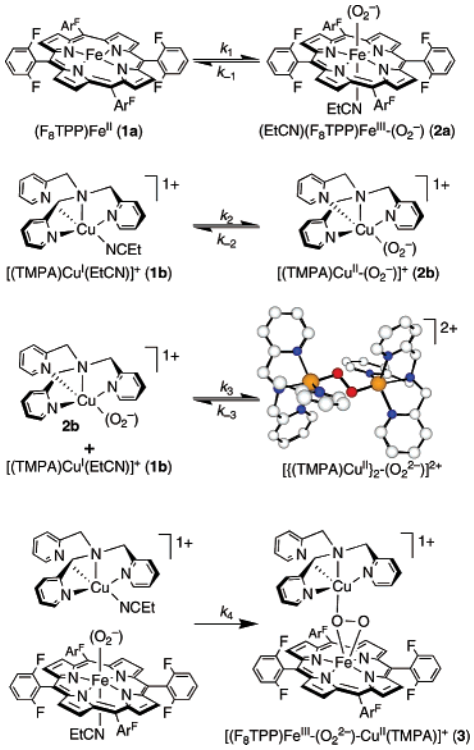

enthalpy ($\Delta H^{\ddagger} = 27$ kJ/mol) determined for formation of **3** is somewhat lower than that observed for the same complex in acetone as solvent ($\Delta H^{\ddagger} = 45$ kJ/mol), or values determined for other complexes (Table 6). There are too many variables (i.e., solvent and metal−solvate dissociation chemistry, copper−ligand denticity, inter- vs intramolecular reactions) to make firm conclusions concerning the reason for this. Nevertheless, a likely explanation is the Cu^{I}−TMPA moiety, with its tetradentate chelate, is significantly more reducing than Cu^{I} in any of the other systems (Table 6), providing facilitated reaction with the $Fe^{III}-O_2^-$ intermediate resulting in formation of heme−peroxo−Cu complex **3**. In **IV** (Chart 1), the copper environment is a distorted tetradentate (more like tridentate),[20,74] while for **V**−**VI**, tridentate ligands are involved. Recent[75] redox potential measurements with copper(I) complexes of these tri- and tetradentate pyridylalkylamine-containing ligands support the supposition concerning relative reducing power.

Mössbauer Evidence Supporting the Presence of a Heme−Superoxo Intermediate. The oxygenation reaction of **1a**/**1b** in acetone at −80 °C was also studied by Mössbauer spectroscopy. Figure 10A displays a Mössbauer spectrum of the starting material **1a**/**1b** before introduction of oxygen. The spectrum, which was recorded at 4.2 K in the absence of a magnetic field, shows a quadrupole doublet with parameters ($\Delta E_Q = 2.66$ mm/s and $\delta = 0.93$ mm/s) that are typical for high-spin ferrous heme compounds. Since high-spin ferrous heme compounds are generally five-coordinate, this observation suggests the presence of an axial ligand,

(74) Ju, T. D.; Ghiladi, R. A.; Lee, D.-H.; van Strijdonck, G. P. F.; Woods, A. S.; Cotter, R. J.; Young, J., V. G.; Karlin, K. D. *Inorg. Chem.* **1999**, *38*, 2244−2245.
(75) Osako, T.; Karlin, K. D.; Itoh, S. *Inorg. Chem.* **2005**, *44*, 410−415.

Table 6. Kinetic Parameters for the Formation of Heme−Peroxo−Copper Complexes from Reaction of Initially Formed (P)Fe^{III}−(O_2^-) Intermediates with Ligand−Cu(I) Moieties

heme−peroxo−copper complex	*k*	$\Delta H^{\ddagger}$ (kJ/mol)	$\Delta S^{\ddagger}$ (J/mol·K)
[(F_8TPP)Fe^{III}−(O_2^{2-})−Cu^{II}(TMPA)]$^+$ (**3**)[a]	$k_4 = (2.77 \pm 0.05) \times 10^4$ (M^{-1} s^{-1}) (183 K)[b] $k_4 = (7.2 \pm 0.1) \times 10^4$ (M^{-1} s^{-1}) (193 K)[b] $k_4 = (1.70 \pm 0.05) \times 10^5$ (M^{-1} s^{-1}) (203 K)[b]	26.5 ± 0.6	−11 ± 3
	0.07 s^{-1} (183 K)[c,21] 0.32 s^{-1} (193 K)[c,21]	45 ± 1	−19 ± 6
[(^{6}L)Fe^{III}−(O_2^{2-})−Cu^{II}]$^+$ (**IV**)[22]	2.55 s^{-1} (183 K)[d] 9.62 s^{-1} (193 K)[d] 31.9 s^{-1} (203 K)[d]	37.4 ± 0.4	−29 ± 2
[(^{2}L)Fe^{III}−(O_2^{2-})−Cu^{II}]$^+$ (**V**)[23]	$(2.74 \pm 0.04) \times 10^1$ s^{-1} (168 K)[e] $(2.55 \pm 0.03) \times 10^2$ s^{-1} (183 K)[e] $(1.70 \pm 0.05) \times 10^3$ s^{-1} (198 K)[e]	36.6 ± 0.4	5 ± 2
[(F_8TPP)Fe^{III}−(O_2^{2-})−Cu^{II}(L^{Me2N})]$^+$ (**VI**) [25]	$(1.28 \pm 0.03) \times 10^4$ (M^{-1} s^{-1}) (168 K)[e] $(1.16 \pm 0.01) \times 10^5$ (M^{-1} s^{-1}) (183 K)[e] $(7.6 \pm 0.1) \times 10^5$ (M^{-1} s^{-1}) (198 K)[e]	36.2 ± 0.2	54 ± 1

[a] This work. [b] EtCN solvent. [c] Acetone, pseudo-first-order rate constants for [metal−complex] = 2.71×10^{-4} M, [O_2] = 2.55×10^{-3} M at RT (calculated from the thermodynamic data in ref 21). [d] Acetone solvent, calculated from the thermodynamic data in ref 22. [e] 6% EtCN/CH_2Cl_2.

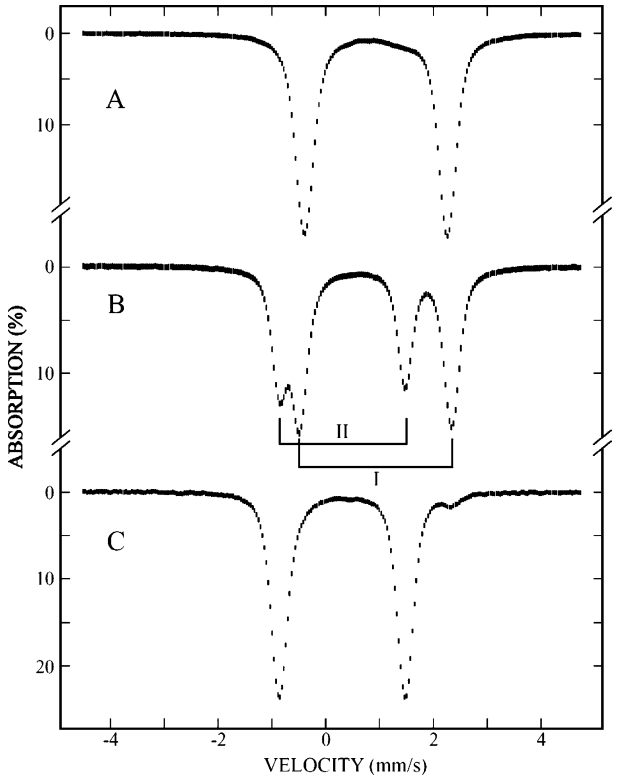

Figure 10. Oxygenation reaction of (F_8TPP)Fe^{II}/[(TMPA)Cu^{I}(MeCN)]$^+$ (**1a**/**1b**) in acetone monitored by Mössbauer spectroscopy. The spectra were recorded at 4.2 K and in the absence of a magnetic field. Spectrum A was taken prior to the addition of O_2, and spectrum B was recorded from a sample frozen ∼10 s after the addition of oxygen. Reacting O_2 with **1a** in the absence of **1b** resulted in spectrum C, corresponding to quadrupole doublet II of spectrum B, see text.

most likely a solvent molecule, for **1a** in acetone. This situation has already been described on the basis of ^{1}H or ^{2}H NMR spectroscopic studies.[27] After the addition of dioxygen, the sample was rapidly (∼10 s) frozen in liquid nitrogen and investigated by Mössbauer spectroscopy. Figure 10B shows a spectrum of the oxygen-reacted sample recorded at 4.2 K in zero field. Two well-resolved quadrupole doublets, marked by brackets I and II, are observed. Doublet I, accounting for 63% of the total iron absorption, exhibits parameters (ΔE_Q = 2.82 mm/s and δ = 0.93 mm/s) that are similar to those of the starting materials and thus represents the unreacted **1a**. Doublet II accounts for 37% of the total iron absorption and exhibits characteristic parameters (ΔE_Q = 2.33 mm/s and δ = 0.31 mm/s) that are commonly observed for O_2-bound ferrous heme compounds, such as oxygenated myoglobin and hemoglobin, of which the oxidation state may be formulated as Fe^{III}−O_2^-.[76] As a control, we also reacted **1a** with dioxygen in the absence of **1b** in acetone, known to give **2a**.[27] A Mössbauer spectrum of the O_2-reacted **1a** sample recorded at 4.2 K in the absence of a magnetic field (Figure 10C) showed a quadrupole doublet identical to doublet II. Taken together, the Mössbauer data presented here and the UV−visible stopped-flow data presented above demonstrate unambiguously that a ferric heme−superoxo **2a** intermediate is present as a precursor of **3** in the O_2 reaction of **1a**/**1b** (Scheme 1).

Thermal Rearrangement of 3 to 4. The thermal decomposition of μ-peroxo complex **3** to μ-oxo complex **4** was found to be slow {$t_{1/2}$ = 1016 ± 20 s; MeCN, 22 °C, 0.28 mM} as determined by benchtop UV−visible spectroscopy.[21] The question then arises as to the fate of the second oxygen atom apparently lost during this transformation. Does **3** undergo O-atom transfer to a substrate, i.e., solvent, exhibiting monooxygenase activity? Or, as an alternative, is dioxygen liberated during this decomposition process, similar to the situation found for the analogue compound **IV** (Chart 1)?[20]

To answer the latter, alkaline pyrogallol, a known dioxygen scavenger, was used in a colorometric assay (as previously described) to detect and quantify evolved dioxygen gas.[20,23] The results indicated 0.4−0.46 equiv of dioxygen were evolved during the formation of **4**. Thus, no loss of oxygen (to solvent oxidation, perhaps) occurred. As depicted in Scheme 1, 1 equiv of dioxygen reacts with reduced precursors to form peroxo complex **3**, but some type of disproportionation reaction occurs in the thermal transformation to μ-oxo complex **4**, and 0.5 equiv of O_2 is evolved. We have not been able to obtain mechanistic insights into this interesting reaction but have elsewhere[20] provided a detailed discussion about such disproportionation reactions, known for heme and non-heme iron systems.

(76) Weiss, J. J. *Nature* **1964**, *203*, 182−183.

Summary/Conclusions

We have demonstrated that oxygenation of a simple mixture of the heme and copper complexes **1a** and **1b** forms the heterobinuclear complex **3**. This possesses an unsymmetrical side-on/end-on μ-η^2:η^1-peroxo coordination, as further supported by the present rR spectroscopic finding of two distinct $Fe^{III}-O$ stretching vibrations. As previously inferred from magnetic moment measurements (Evans method), as well as the distinctive pattern of ^1H NMR downfield-shifted pyrrole and upfield-shifted pyridyl hydrogen resonances, **3** is an antiferromagnetically coupled (Fe(III) and Cu(II)) $S = 2$ spin system; as presented in this report, ^2H NMR measurements along with Mössbauer spectroscopic investigations confirm these conclusions. We also probed the properties of **3** and **4** using ^{19}F NMR spectroscopy; a comparison of data to those known for other species (e.g., heme−superoxo complex **2a** and peroxo species $\{(F_8TPP)Fe^{III}\}_2(O_2^{2-})$) reveals useful empirical correlations based on compound magnetic properties.

Stopped-flow spectrophotometry and Mössbauer spectroscopy reveal the formation of a heme−superoxo complex (**2a**) as a precursor to forming **3**, a result seen previously for the oxygenation of other $PFe^{II}Cu^{I}$ complexes, with dioxygen-uptake experiments confirming that the formation of the peroxide bridge in **3** occurs upon addition of 1 equiv (per Fe^{II}/Cu^{I} heterobinuclear center) of dioxygen. Thermal transformation of peroxo species **3** to μ-oxo complex **4** occurs with concomitant release of 0.5 equiv of dioxygen; the mechanism of this disproportionation and O−O bond cleavage reaction deserves further attention.

While possessing quite detailed characterization of the chemistry of high-spin μ-peroxo complexes **3**, close relative **IV** (Chart 1), Naurta's peroxo complex (**III**, Chart 1), and even the analogues with tridentate ligands for copper (**V** and **VI,** Chart 1), additional insights are warranted. For example, can a high-spin ($S = 2$) heme−peroxo−Cu complex be converted to low-spin, either by addition of a strong field axial base or through changes in the nature of the starting Fe^{II}/Cu^{I} complex(es)? Can similar heme−peroxo−Cu complexes be formed from addition of (ligand)Cu^{II} (tetra- and tridentate ligands) compounds to side-on peroxo species $[(P)Fe^{III}-(O_2^{2-})]^-$?[77] Can any such $Fe-O_2-Cu$ complexes be subjected to conditions which lead to reductive O−O bond cleavage, by addition of proton/electron sources, in order to probe this reaction which is key to cytochrome oxidase function and in general for metal ion mediated O_2-activation? Studies related to these matters are in progress.

Acknowledgment. We are grateful to the National Institutes of Health (K.D.K., GM60353; R.J.C., GM54882; P.M.-L., GM34468 to Prof. T. M. Loehr; B.H.H., GM47295; E.I.S., DK31450) and the Swiss National Science Foundation (A.D.Z.) for support of this research. D.R. thanks the sixth Framework program of the EU for a MC-OIF fellowship.

Supporting Information Available: Synthesis of $(F_8TPP)^{57}Fe^{II}$ (**1a-^{57}Fe**), UV−visible spectra of the $(F_8TPP)Fe^{II}/[(TMPA)Cu^{I}(MeCN)]^+$ (**1a/1b**) oxygenation reaction (Figure S1), discussion and data for the O_2-uptake of **1a/1b** by means of a UV−visible-monitored spectrophotometric titration (Figure S2), resonance Raman spectra of $[(F_8TPP)Fe^{III}-(O_2^{2-})-Cu^{II}(TMPA)]^+$ (**3**) (Figure S3), calculated effects of splitting the 810 cm^{-1} O−O stretch (Figure S4), calculated effect of splitting in the 920 cm^{-1} solvent vibration (Figure S5), resonance Raman spectra of **3** obtained with a 775 nm excitation (Figure S6), schematic representation of atom displacement from the normal coordinate analysis of the μ-η^2:η^1 $Fe-O_2-Cu$ core structure (Figure S7), and atom displacement matrix (for the $^{16}O_2$ isotopomer) (Table S1), Mössbauer spectra of $[(F_8TPP)Fe^{III}-O-Cu^{II}(TMPA)]^+$ (**4**) (Figure S8), kinetic trace for formation of $(EtCN)(F_8TPP)Fe^{III}-(O_2^{-})$ (**2a**) followed by its transformation to $[(F_8TPP)Fe^{III}-(O_2^{2-})-Cu^{II}(TMPA)]^+$ (**3**) (Figure S9), Eyring plot for the formation of $[(F_8TPP)Fe^{III}-(O_2^{2-})-Cu^{II}(TMPA)]^+$ (**3**) in EtCN (Figure S10), and experimental details for the alkaline pyrogallol detection of evolved dioxygen during the thermal rearrangement of **3** to **4**. This material is available free of charge via the Internet at http://pubs.acs.org.

IC061726K

(77) Chufán, E. E.; Karlin, K. D. *J. Am Chem. Soc.* **2003**, *125*, 16160−16161.